ASTRONOMICAL CONSTRAINTS ON THE DURATION OF THE EARLY JURASSIC PLIENSBACHIAN STAGE AND GLOBAL CLIMATIC FLUCTUATIONS

MICHA RUHL[1], STEPHEN P. HESSELBO[1,2], LINDA HINNOV[3], HUGH C. JENKYNS[1], WEIMU XU[1], MARISA STORM[1], JAMES B. RIDING[4], DANIEL MINISINI[5], CLEMENS V. ULLMANN[2], MELANIE J. LENG[4,6]

[1] Department of Earth Sciences, University of Oxford, South Parks Road, Oxford OX13AN, UK
[2] Camborne School of Mines, University of Exeter, Penryn TR10 9FE, UK
[3] Department of Atmospheric, Oceanic and Earth Sciences, George Mason University, Fairfax Campus, 4400 University Drive, Fairfax, VA 22030, Virginia, USA
[4] British Geological Survey, Keyworth, Nottingham NG12 5GG, UK
[5] Shell Exploration and Production Incorporated, Shell Houston Technology Center, 3333 Highway 6 South, Houston, TX 77082, Texas, USA
[6] School of Geography, University of Nottingham, University Park, Nottingham NG7 2RD, UK

Keywords: *astrochronology, carbon-cycle, cyclostratigraphy, Early Jurassic, Pliensbachian, strontium isotopes*

ABSTRACT

The Early Jurassic Epoch was marked by multiple periods of major global climatic and palaeoceanographic change, biotic turnover and perturbed global geochemical cycles, commonly linked to large igneous province volcanism. This interval was also characterized by the initial break-up of the supercontinent Pangaea and the opening and formation of shallow-marine basins and ocean gateways, the timing of which are still poorly constrained. Here, we show that the

Pliensbachian Stage and the Sinemurian–Pliensbachian global carbon-cycle perturbation (marked by a negative shift in $\delta^{13}C$ of 2–4‰), have respective durations of ~8.7 and ~2 Myr. We astronomically tune the floating Pliensbachian time scale to the 405 kyr eccentricity solution (La2010d), and propose a revised Early Jurassic time-scale with a significantly shortened Sinemurian Stage of 6.9 ± 0.4 Myr. When calibrated against the new time scale, the existing Pliensbachian seawater $^{87}Sr/^{86}Sr$ record shows relatively stable values during the first ~2 Myr of the Pliensbachian, superimposed on the long-term Early Jurassic decline in $^{87}Sr/^{86}Sr$. This plateau in $^{87}Sr/^{86}Sr$ values coincides with the Sinemurian–Pliensbachian boundary carbon-cycle perturbation. It is possibly linked to a late phase of Central Atlantic Magmatic Province (CAMP) volcanism that induced enhanced global weathering of continental crustal materials, leading to an elevated radiogenic strontium flux to the global ocean.

[1] INTRODUCTION

The Early Jurassic (201.4–174.1 Ma) is distinguished by the end-Triassic mass extinction and global warming event, climatic cooling in the Late Pliensbachian and subsequent greenhouse warming in the Early Toarcian (McElwain et al., 1999; Hesselbo et al., 2002; Ruhl et al., 2011; Gradstein et al., 2012; Wotzlaw et al., 2014; Gomez et al., 2015; Korte et al., 2015). The Early Toarcian was characterized by the global Toarcian Oceanic Anoxic Event (T–OAE), with possibly the largest exogenic carbon-cycle perturbation in the Mesozoic, and consequential perturbations in other global geochemical cycles, climate and the environment, which has been linked to emplacement of a large igneous province (LIP) in the Karoo-Ferrar region (Jenkyns, 2010; Burgess et al., 2015).

Early Jurassic continental rifting and the break-up of Pangaea led to the formation of continental and marine rift basins, which acted as major sinks for the burial of organic carbon and the generation of hydrocarbon source rocks (Olsen, 1997). The equatorial Tethys Ocean was linked in the Early Jurassic (Sinemurian) to Eastern Panthalassa via the Hispanic Corridor and to the high-latitude Arctic Boreal realm via the Viking Strait, likely initiating changes in global ocean currents and planetary heat distribution (Figure 1; Porter et al., 2013; Korte et al., 2015).

The Early Jurassic was also marked by further fluctuations in the global exogenic carbon cycle (Riding et al., 2013; Jenkyns and Weedon, 2013), shifts between climatic warming and cooling on regional and global scale (Korte et al., 2009; Korte and Hesselbo, 2011; Korte et al., 2015), marine and continental extinction and origination events (Close et al., 2015), and fluctuations in regional and global sea-level (Hallam, 1997; Hesselbo et al., 2004, 2008). MICHA – THE PREVIOUS SENTENCE IS VERY COMPLEX - ?CONSIDER PUTTING ALL THE REFERENCES AT THE END? The age, rate of change, and duration of these events are, however, poorly constrained and their inter-relationships only crudely appreciated.

Here, we constrain the age and duration of the Early Jurassic Pliensbachian Stage and zones and subzones in the hemipelagic marine sedimentary record of the Mochras Farm (Llanbedr) Borehole from west Wales (Cardigan Bay Basin). The Mochras Borehole represents ~1300 m of possibly the most continuously deposited and stratigraphically expanded Lower Jurassic sedimentary archive known (Figure 2; Hesselbo et al., 2013). High-resolution (sub-precession scale) element concentration data are used to construct a floating astronomical time scale for the Early Jurassic Pliensbachian Stage. Combined with published astrochronological and radiometric constraints on the age of the Rhaetian–Hettangian (Triassic–Jurassic) and Pliensbachian–Toarcian stage boundaries, and astrochronological constraints on the duration of the Hettangian and Toarcian stages, we calculate the duration and age of the Pliensbachian stage and its constituent zones. With these data, we then assess the duration and rate of change of the

Sinemurian–Pliensbachian climatic and global carbon-cycle perturbations and the Late Pliensbachian climatic cooling cycles, and assess the rate of change of Pliensbachian seawater $^{87}Sr/^{86}Sr$.

[2] THE MOCHRAS FARM (LLANBEDR) BOREHOLE

The Mochras Farm (Llanbedr) Borehole, hereafter referred to as Mochras core, was drilled in 1968–1970 on the west coast of Wales (52°48'32" N, 4°08'44" W; Figure 1; Woodland, 1971; Dobson and Whittington, 1987; Hesselbo et al., 2013; Copestake and Johnson, 2013). The borehole yielded, unexpectedly, a ~1.3 km-thick (601.83–1906.78 m below surface), biostratigraphically complete succession of calcareous mudstone and clay-rich limestone, representing almost the complete Lower Jurassic, an interval representing some 27 Myr of geological time. The Lower Jurassic sedimentary record in the Mochras core is more than twice as thick as any other UK core or coastal outcrop, and is over four times more expanded than the well-studied Sancerre–Couy core from the Paris Basin, France (Figure 2; Tappin et al., 1994; Hesselbo et al., 2013; Boulila et al., 2014). The Hettangian and Sinemurian part of the Mochras core was largely broken up for biostratigraphical sampling; hence only limited continuous core is preserved for these stages. Continuous core-slabs are, however, preserved for the Pliensbachian and Toarcian part of the Mochras core (Hesselbo et al., 2013).

[3] BIO- AND CHEMOSTRATIGRAPHY

Biostratigraphical zones, combined with high-resolution geochemical proxy records, provide the primary means for global correlation of Lower Jurassic marine and terrestrial sedimentary archives. The Pliensbachian Stage in northwest Europe is subdivided into five ammonite zones (and 15 ammonite subzones), which are all present and recognized in the Mochras core (Ivimey-Cook, 1971; Page, 2003; Copestake and Johnson 2013). In this paper, these are referred to as zones and subzones, and are named by the index species name only (e.g. *margaritatus* zone). Foraminifera provide further biostratigraphical constraints on the core, and allow detailed correlation to records elsewhere (Copestake and Johnson, 2013).

The Pliensbachian is further marked by perturbations of global geochemical cycles and climate. A 2–4‰ negative shift in the carbon-isotope composition ($\delta^{13}C$) of both skeletal (belemnite) calcite, bulk shallow-water carbonate and organic matter is recognized at the Sinemurian–Pliensbachian boundary at Robin Hood's Bay (Yorkshire, UK), the Central Apennines and Trento Platform (Italy), in Portugal and Germany, and in the Mochras core (Jenkyns et al., 2002; Morettini et al., 2002; van de Schootbrugge et al., 2005; Korte and Hesselbo, 2011; Franceschi et al., 2014). This negative carbon-isotope excursion (CIE) likely represents a global carbon-cycle perturbation (with associated climatic change), and allows detailed stratigraphical correlation, potentially at a resolution equivalent to, or even significantly higher than, ammonite zones. The Late Pliensbachian was marked by a major positive shift (of up to 5‰) in the $\delta^{13}C$ of wood ($\delta^{13}C_{WOOD}$) and up to 3‰ in the $\delta^{13}C$ of organic matter ($\delta^{13}C_{TOC}$; TOC: Total Organic Carbon) (Figure 7; Suan et al., 2010; Korte & Hesselbo, 2011; Silva et al., 2011), reflecting enrichment of ^{13}C in the coupled ocean-atmosphere carbon pool (and thus a perturbation of the global carbon cycle). This carbon-cycle perturbation in the upper *margaritatus* zone, coincides with regionally identified sea-level fluctuations and associated changes in shallow-marine $\delta^{18}O_{CALCITE}$, possibly reflecting climatic cooling cycles under conditions of massive carbon burial, with an enhanced flux of organic matter from the ocean-atmosphere system to the sedimentary carbon pool (Korte and Hesselbo, 2011). Alternatively, regional cooling may have resulted from an early phase of obstruction of the Viking corridor, leading to decreased seawater temperatures across northwest Europe (Korte et al., 2015). The observed Pliensbachian perturbations in global geochemical cycles allow for detailed high-resolution stratigraphical correlation between geographically separated sedimentary archives from both the marine and terrestrial realms.

[4] ANALYTICAL METHODS

High-resolution (10–15 cm) elemental concentrations (e.g. Ca, Fe, Ti) MICHA – I PUT THE PREVIOUS ELEMENTS IN ABC ORDER. were obtained by hand-held X-ray fluorescence (XRF) analyses on the slabbed archive half of the Mochras core, from the Late Sinemurian *raricostatum* zone to the Early Toarcian *tenuicostatum* zone (1284.08–861.32 m). Rock-Eval analysis, providing Total Organic Carbon (TOC) content, Hydrogen Index (HI) values and % Mineral Carbon, was performed on ~50 mg of homogenized sample, with the Rock-Eval VI unit from Vinci Technologies, at the department of Earth Sciences, University of Oxford. Analysis of $\delta^{13}C_{TOC}$ was performed on decarbonated and homogenized Upper Pliensbachian outcrop samples from Staithes (Yorkshire, UK), utilising ammonite biostratigraphy for correlation to the Mochras core (Figure 7). Detailed methodology and data quality control are described in the Supplementary Online Materials.

[5] RESULTS AND DISCUSSION

[5.1] SEDIMENTARY RHYTHMS IN THE PLIENSBACHIAN OF THE MOCHRAS CORE

The Pliensbachian in the Mochras core shows metre-scale lithological couplets of pale grey limestone and dark brown to grey, locally faintly laminated, mudstone, with individual couplets commonly showing gradual transitions between these end-members (Figure 3). The lithological expression of these couplets does, however, vary, in some cases being represented by calcareous mudstones (commonly also more silty) alternating with locally darker, shaly mudstone. The principal lithological variation (the couplets) between carbonate-poor mudstone with moderate organic-matter content (TOC: ~0.9–2.1%) and carbonate-rich mudstone or limestone ($CaCO_3$: ~10–65%) with reduced organic-matter content, is especially pronounced at the Sinemurian–Pliensbachian transition (base *jamesoni* zone) and the top *ibex* to base *margaritatus* zones (Figures 3, 4; Supplementary Figure 2). Primary lithological cycles occur throughout the Pliensbachian in the Mochras core, and vary in thickness between ~30 cm (i.e. uppermost Pliensbachian) and ~90 cm (i.e. Lower Pliensbachian), with individual carbonate beds measuring 20–40 cm (reduced to 5–20 cm in the Upper Pliensbachian) (Figures 3, 4).

Individual lithological couplets are generally symmetrical in nature, with little indication of depositional hiatuses or scouring (Figure 3). The more organic-rich lithology is commonly dark grey and faintly (millimetre-scale) laminated, particularly in the lowermost Pliensbachian part of the core, whereas the more carbonate-rich lithology is commonly thoroughly bioturbated (Figure 3). Thin-section analysis shows evidence for minor early diagenetic processes, such as calcite replacement and cementation (Supplementary Figure 3), possibly resulting from the degradation of organic matter and the associated reduction of sulphate, as evidenced by the occurrence of pyrite framboids. However, we exclude the possibility that the lithological couplets are solely related to diagenesis, and interpret them as depositional in origin, as supported by the burrow mottling, with dark-pale and pale-dark mixing of primary sediments (cf. Hallam, 1986). Furthermore, variation in HI of the bulk sedimentary organic matter closely matches the observed variations in $CaCO_3$, further suggesting a climatic control on periodic fluctuations in the supply of organic and inorganic matter to the sea bed (Supplementary Figure 2), similar to that observed for the Kimmeridge Clay Formation at Kimmeridge Bay (UK) and the Blue Lias Formation at Lyme Regis and in Somerset (UK) (Weedon, 1985; Waterhouse, 1999; Weedon et al., 1999; Clemence et al., 2010; Ruhl et al., 2010). Alternatively, observed drops in HI values may have resulted from the oxidative removal of marine algal organic matter in better-oxygenated conditions in the water column and/or sedimentary pore space. Lithological couplets of similar character have also been observed for coeval Pliensbachian successions in other marine basins across the UK (e.g. Sellwood, 1970, 1972; van Buchem et al., 1989, 1992; Hesselbo and Jenkyns 1995; Weedon and Jenkyns, 1999). For example, lithological changes in the Mochras core closely resemble the time-equivalent Belemnite Marl Member (Charmouth Mudstone Formation) in outcrops on the Dorset coast, where individual beds and distinct calcareous mudstone-shale couplets are laterally continuous for over 2 km (Weedon & Jenkyns, 1999), suggesting chronostratigraphical significance and a stable allogenic forcing mechanism, likely to be high-frequency climate change. The uppermost Sinemurian and Pliensbachian sedimentary sequence in the Mochras core also shows similar periodic alternations in lithology relative to the coeval shallow-marine Redcar Mudstone Formation at Robin Hood's Bay, although these latter sediments are characterised by silty to very fine sandy mudstone beds alternating with silty mudstone and shale, with common levels of concretionary siderite (van Buchum & McCave, 1989; van Buchem et al., 1992; Hesselbo and Jenkyns 1995; Van Buchem and Knox, 1998).

[5.2] MILANKOVITCH-CONTROLLED SEDIMENTARY PERIODICITIES IN THE PLIENSBACHIAN OF THE MOCHRAS CORE

The observed decimetre- to metre-scale amplitudinal change in calcium concentrations determined by XRF directly reflects the observed lithological couplets (in $CaCO_3$) and are especially prominent around the Sinemurian–Pliensbachian boundary (*raricostatum* and *jamesoni* zones) and in the upper Pliensbachian *margaritatus* zone (Figures 3, 4), illustrating a strong modulation by long-term periodicities. Iron (Fe) and titanium (Ti) concentrations in the Mochras core also strongly fluctuate and are largely negatively correlated with the calcium concentration (Figure 3), suggesting simple sedimentary carbonate dilution. However, different climatic controls on detrital element supply or diagenetic element enrichment may also have affected the carbonate-silicate balance. Early diagenesis was probably only a minor control on the distribution of $CaCO_3$, given the observed burrow mottling (see above). The observed fluctuations in calcium concentrations therefore likely reflect relative changes in the particulate carbonate flux, possibly over Milankovitch frequencies.

The XRF-based Ca-concentration data series, combined with the stacked core photos, allow for the initial visual identification of calcareous beds and associated lithological couplets. These lithological couplets are not evenly spaced, but occur in bundles (E^1) of 4–5 sedimentary rhythms. Within a bundle the more calcareous beds generally thicken up-section and become more pronounced, forming a weakly asymmetric cycle (Figures 3, 4). Generally four of these smaller bundles (E^1), each consisting of 4–5 lithological couplets, occur in one super-bundle (E^2). The observed couplets, bundles (E^1) and super-bundles (E^2) can generally be recognized throughout the core, but vary in thickness, probably due to minor changes in sedimentation rate (Figure 4). The ratio between the thickness of the couplets, the bundles and the super-bundles is, however, constant, suggesting a stable forcing mechanism, presumably high-frequency climatic control operating on Milankovitch frequencies. The lithological couplets in the coeval Belemnite Marls in Dorset are suggested to represent ~21 kyr precession cyclicity (Weedon & Jenkyns, 1999). Following this interpretation, we assign ~100 and ~405 kyr eccentricity periodicities to the visually defined bundles (E^1) and super-bundles (E^2) (Figures 3, 4). This procedure allows for independent comparison to Milankovitch periodicities assigned from subsequent spectral and multi-taper analyses. Some of the E^1-bundles are, however, marked by only two lithological couplets that are generally thicker and more carbonate-rich, and which consistently occur only during the minima between two E^2-bundles (Figure 4). Following the above, they may reflect a change from dominant eccentricity-modulated precession forcing to obliquity forcing.

[5.3] SPECTRAL & MULTI-TAPER ANALYSES

The XRF elemental data obtained from the Pliensbachian of the Mochras core were manipulated to uniform sample spacing using linear interpolation. For spectral analyses, the series were analyzed with the 3π multi-taper method (MTM) using the Astrochron toolkit (Meyers, 2014; R Package for astrochronology, version 0.3.1), with robust red noise models (Mann and Lees, 1996), and with AnalySeries 2.0.8 (Paillard et al., 1996). AGAIN, WOULD THIS SENTENCE READ BETTER WITH ALL THE REFERENCES AT THE END?

Initial spectral analysis was performed with AnalySeries on a detrended data-series (with low band-pass filtering to remove periodicities>150 m). Dominant spectral components (Supplementary Figure 4) were filtered from the data series, and compared to the visually defined precession (lithological couplets) and long- and short-term eccentricity periodicities (Figure 4). The data-series in the depth domain was subsequently converted into a time-series, based on the observed and interpreted dominant ~405 kyr eccentricity cycle. Low-frequency band-pass filtering was then performed with Astrochron on the raw-data time-series to remove long-term trends. High-precision extraction of dominant spectral components (Figure 5, Supplementary Figures 4, 5, 6), with long- and short-term cycles of eccentricity, obliquity and precession, were subsequently extracted with Taner bandpass filtering (Astrochron) and Analyseries.

The MTM power spectrum estimates of the Ca-concentration in the depth domain, show dominance of the >150 m spectral peak (Supplementary Figure 4-A). Removal of this long-term trend by high band-pass filtering shows dominant spectral components at ~1, ~1.5, ~2.5, ~5.8 and ~24 m (Supplementary Figure 4-B). Lithological observations and visually described changes in Ca-concentrations show a pronounced reduction in thickness of the observed lithological couplets, relative to the underlying Pliensbachian strata, in the upper *margaritatus* and complete *spinatum* zones (Figure 4). Individual couplets, however, continued to be spaced in the observed bundles (E^1) and super-bundles (E^2), and lack any evidence of periodic hiatuses. The reduced thickness of individual couplets, combined with the continued bundling, suggests an overall reduced sedimentation rate in this part of the Mochras core.

Individual MTM power spectra for the uppermost *raricostatum* to lower *margaritatus* and the upper *margaritatus* to lowermost *tenuicostatum* zones (Supplementary Figures 4-C, D, respectively), indeed show that dominant spectral components occur at different frequencies, but with equal internal ratios suggesting a ~40–60% reduction in sedimentation rate (Supplementary Figure 7). The ~1 and ~0.6 m spectral components in these intervals directly reflect the observed primary sedimentary rhythms, recognized throughout the Pliensbachian of the Mochras core (Figure 4). The observed dominant spectral peaks directly reflect the visually ascribed individual lithological rhythms and bundles (E^1) and super-bundles (E^2) where carbonate predominates, likely representing precession and short- and long-term eccentricity. Using this assumption, the sedimentary and geochemical records of the Mochras core can be converted to a time-series. This floating astronomical time-scale for the Early Jurassic may also be reliably tuned to the proposed astronomical solutions for this time period (e.g. Laskar et al., 2011), using radiometric tie points.

[5.4] ASTRONOMICAL CONSTRAINTS ON THE DURATION OF THE PLIENSBACHIAN STAGE AND ZONES

The base of the Pliensbachian is formally defined by a mudstone bed in the Pyritous Shale Member (Redcar Mudstone Formation) at Robin Hood's Bay, Yorkshire, UK, marked by the lowermost occurrence of the ammonite species *Bifericeras donovani*; with additional stratigraphical markers including a brief reversed-polarity magnetozone (at the base of Si-Pl N) and a negative excursion in $\delta^{13}C$ (Hesselbo et al. 2000, Meister et al., 2006; Korte and Hesselbo, 2011). The Pliensbachian Stage is conventionally divided into the lower (Carixian) and upper (Domerian) substages and, at a higher resolution, into ammonite zones. Some authors, e.g. Page (2004), prefer to treat ammonite-based subdivisions as chronozones rather than biozones or zones but, given the absence of corroboration of their time significance, we treat them as conventional biostratigraphical units. These are successions of sedimentary rock characterised by specific fossil assemblages, and defined to be (closely) approximate in depositional age and hence are characteristic of specific time intervals.

The observed variation in stratigraphical spacing of lithological couplets, and the recognition of bundles (E^1) and super-bundles (E^2), combined with spectral and multi-taper analyses showing dominant frequencies in high-resolution geochemical records, suggest Milankovitch (astronomical) control on sedimentary deposition. The relative frequency of different-order lithological changes and comparison with the Belemnite Marls in Dorset suggest that the primary lithological rhythms (couplets), bundles (E^1) and super-bundles (E^2) in the Mochras core reflect precessional forcing, modulated by ~100 and ~405 kyr eccentricity forcing (Figures 3, 4). The visual core observations and interpretations, combined with the spectral and multi-taper analyses of geochemical records, together with the precise biostratigraphical subdivision of the Mochras core, can be taken to estimate the duration of Pliensbachian ammonite zones. The precision of the estimates obtained for ammonite zone durations depends on (1) the correct recognition of the dominant orbital signals, and (2) the uncertainty of the precise position of the stratigraphical base of an ammonite zone in the core. Here, we derive ammonite zone durations based on the observed 405 and ~100 kyr forcing in the geochemical proxy-records. The stratigraphical occurrences of ammonite taxa identified in the Upper Sinemurian to Lower Toarcian of the Mochras core, which are used to define the ammonite zones, is given in Supplementary Figure 7. The base of individual ammonite zones is based on the first occurrence, in the core, of a specific ammonite genus, which often directly follows the last occurrence, in the core, of the ammonite genus defining the preceding ammonite zone (Supplementary Figure 7). The temporal or stratigraphical uncertainty on the base of ammonite zones, relative to for example outcrop successions is presently, however, impossible to assess. Given the above, resulting ammonite zone durations are estimated at ~2.7 Myr (*jamesoni*), ~1.8 Myr (*ibex*), ~0.4 Myr (*davoei*), ~2.4 Myr (*margaritatus*) and ~1.4 Myr (*spinatum*), yielding a duration of the complete Pliensbachian Stage of ~8.7 Myr (Figure 4; Table 1).

The durations estimated here for the *jamesoni* and *ibex* zones are significantly longer than previous (minimum) estimates from the Belemnite Marls (Dorset) and the Ironstone Shale (Yorkshire) (van Buchem et al., 1989; Hesselbo and Jenkyns, 1995; Weedon & Jenkyns, 1999). The base and top of the Belemnite Marl Formation (representing the base of the *jamesoni* zone and the top of the *ibex* zone in the Dorset outcrops) are marked by stratigraphical gaps (Hesselbo and Jenkyns, 1995; Weedon and Jenkyns, 1999), likely explaining their shorter estimated durations. The likely underestimated durations of Early Pliensbachian ammonite zones based on the Belemnite Marls sedimentary sequence, is furthermore suggested by time-series analyses of the Mochras % Ca data imposed onto the Belemnite Marl Early Pliensbachian time-scale (Supplementary Figure 8), which shows spectral peaks that have no correspondence to dominant astronomical frequencies as known from the geological record and astronomical solutions (Supplementary Figure 8). The new duration estimated here for the *davoei* zone is similar to an earlier proposed value from Breggia Gorge (southern Switzerland), which was previously considered to be only 46% complete (Weedon, 1989). The latter was, however, based on the assumption that Jurassic ammonite zones were ~1 Myr in duration and that only 22 of the expected 48 precession cycles could be recognized (Weedon, 1989). Given the similar obtained duration for the *davoei* zone in the Mochras core, where no evidence for a hiatus, condensation, or non-deposition has been observed, we argue that the *davoei* zone in the Breggia Gorge section is likely complete. The estimated durations of the *margaritatu*s and *spinatum* zones are significantly longer, respectively 0.7 and 0.6 Myr, compared to previous minimum estimates of Weedon (1989) and Weedon and Jenkyns (1999). Our estimated duration of ~3.8 Myr for the combined *margaritatu*s–*spinatum* zones does, however, closely resemble previous estimates of ~3.96 Myr based on the assumed rate of change of Early Jurassic seawater $^{87}Sr/^{86}Sr$ (McArthur et al., 2000).

[5.5] TOWARDS AN ABSOLUTE TIME SCALE FOR THE EARLY JURASSIC HETTANGIAN–PLIENSBACHIAN STAGES

Zircon U-Pb radiometric dating of the earliest CAMP (Central Atlantic Magmatic Province) flood basalts in eastern North America and volcaniclastic material in the Pucara Basin (Peru), respectively, anchor the end-Triassic mass extinction at 201.56 ± 0.02 Ma and at 201.51 ± 0.15 Ma (Schoene et al., 2010; Blackburn et al., 2013; Wotzlaw et al., 2014). The age of the Triassic–Jurassic boundary is radiometrically constrained at 201.36 ± 0.17 Ma in the Pucara Basin (Peru) (Schaltegger et al., 2008; Schoene et al., 2010; Wotzlaw et al., 2014) and astrochronologically constrained at 201.42 ± 0.022 Ma in the Newark/Hartford sequence (Blackburn et al., 2013).

The duration of the Hettangian Stage has been previously estimated by cyclostratigraphy at >~1.29 Myr from the relatively incomplete marine Blue Lias Formation succession in Dorset and Devon, SW England, or at ~2.86 Myr based on an assumed constant linear Early Jurassic decrease in seawater $^{87}Sr/^{86}Sr$ ratios (Weedon and Jenkyns, 1999). More recent estimates for this stage suggest a duration of ~1.7−1.9 Myr, based on the astronomical interpretation of periodically occurring laminated black shales and systematic fluctuations in organic and inorganic geochemical proxy records in the relatively expanded Blue Lias Formation in Somerset, SW England (Ruhl et al., 2010; Hüsing et al., 2014). This duration is further supported by palaeomagnetic correlation to the Geomagnetic Polarity Time-Scale (GPTS) of the Newark Basin (USA) (Hüsing et al., 2014), and a 199.43 (±0.10) Ma ^{238}U/^{206}Pb age for the base Sinemurian in the Pucara Basin (Peru) (Schaltegger et al., 2008; Guex et al., 2012). The duration of the Sinemurian Stage was relatively poorly constrained at ~7.62 Myr, based on assumed constant sedimentation rates and a linear decrease in ^{87}Sr/^{86}Sr (Weedon and Jenkyns, 1999).

Acknowledging recognized depositional gaps, earlier astrochronological analyses of the Pliensbachian in Dorset and Yorkshire (UK) and Breggia Gorge (Switzerland), suggested a minimum Pliensbachian Stage duration of 4.82 Myr (Weedon & Jenkyns, 1999 and references therein); adjustment of these data to an assumed linear decrease in seawater ^{87}Sr/^{86}Sr of 0.000042 per Myr for the Belemnite Marls, lengthened this minimum duration of the Pliensbachian Stage to ~6.67 Myr (Weedon & Jenkyns, 1999). The ^{87}Sr/^{86}Sr-based estimate of a ~3.96 Myr long, combined *margaritatus* and *spinatum* zone duration (McArthur et al., 2000), would suggest a much longer duration for the complete Pliensbachian stage.

Absolute age constraints for the base Toarcian are relatively weak. U-Pb radiometric dating of Lower Jurassic volcanic-ashes from the North American Cordillera, integrated with ammonite biochronology, gives ages of 185.7 +0.5/–0.6 Ma for the base of the *kunae* Zone (which slightly precedes the base of the European *margaritatus* zone), 184.1 +1.2/–1.6 Ma for the base of the *carlottense* zone (which is equivalent to the European *spinatum* zone), 183.6 +1.7/–1.1 Ma for the base of the *kanense* zone (which represents the Pliensbachian–Toarcian boundary and which is equivalent to the combined

European *tenuicostatum* and *falciferum* zones), 182.0 +3.3/–1.8 Ma for the base of the *planulata* zone (which is equivalent to the European *bifrons* zone), and 181.4 ±1.2 Ma for the base of the *crassicosta* zone (which slightly post-dates the onset of the European *variabilis* zone) (Pálfy and Smith, 2000). Furthermore, a Re-Os isochron age based on several combined stratigraphical levels in the *falciferum* zone of the Jet Rock (Yorkshire, UK) suggests an age of 178 ±5 Ma for this time-interval (Cohen et al., 2004). The methodological uncertainty on these earlier U-Pb and Re-Os radiometric dates is, however, relatively large, and much larger than one would ideally use for tie-pointing a floating astrochronological time-scale. A bentonite at the base of the *falciferum*-equivalent ammonite zone (*levisoni*-equivalent ammonite subzone) in the Pucara Basin (Peru) was more recently radiometrically (U-Pb) dated at 183.22 ± 0.25 Myr (Sell et al., 2014). The relatively scarce ammonite occurrences in this section, combined with the bio- and chemostratigraphical uncertainty in correlation to the European realm (Guex et al., 2012), however, do also pose a problem for firmly anchoring the Early Toarcian zones to the numerical (absolute) time-scale. For now, this age-estimate, however, probably represents the least uncertain age estimate for this time-interval and it is therefore used here to anchor the top of the Pliensbachian to the numerical time-scale (Figure 6).

The *falciferum* zone follows the lowest Toarcian *tenuicostatum* zone in northwest Europe and the age-equivalent *polymorphum* zone in the Lusitanian Basin (Portugal). The duration of the *polymorphum* (and *tenuicostatum*) zone was astrochronologically constrained to 600–900 kyr in the Lusitanian Basin (Peniche, Portugal; Suan et al., 2008; Huang and Hesselbo, 2014; Ruebsam et al., 2014, 2015), to ~550 kyr in the Lorraine Sub-Basin (France) and to a significantly shorter duration of 90–500 kyr in the Paris Basin Sancerre core (France) (Boulila et al., 2014). The large range in the Sancerre estimate primarily derived from biostratigraphical uncertainty on the exact position of the base Toarcian in that core. Furthermore, the Lower Toarcian sedimentary record in the Lorraine Sub-

Basin and especially also in the Paris Basin is marked by stratigraphical condensation, possibly in response to coeval sea-level change, which compromises the reliability of astrochronological constraints for this time-interval, based on the sedimentary successions of these two basins (Boulila et al., 2014; Ruebsam et al., 2014, 2015). Assuming (1) the 183.22 ± 0.25 Myr radiometric age for the base *falciferum* zone (in the Pucara Basin, Peru; Sell et al., 2014), (2) a synchronous age for the *tenuicostatum–falciferum* zone boundary in north-western Europe, the *kanense–planulata* zone boundary in South America, and the *polymorphum–levisoni* zone boundary in the Lusitanian Basin and (3) a ~600 ± 150 kyr duration for the *polymorphum* (*tenuicostatum*) zone, a 183.8 ± 0.4 Ma age can, tentatively, be assigned to the base of the Toarcian (Figure 6).

The duration of the combined Toarcian *tenuicostatum* and *falciferum* zones is currently much debated, with estimates ranging from ~1.9 Myr (Suan et al., 2008), to ~1.4 or 2.4 Myr (Kemp et al., 2011), ~2.5 Myr (Huang and Hesselbo, 2014), ~1.54–1.71 Myr (Boulila et al., 2014) and >1.8 Myr (Ruebsam et al., 2014, 2015), depending primarily on differences in the precession versus obliquity versus eccentricity interpretation of astronomically forced steps in the Early Toarcian carbon-isotope ($\delta^{13}C$) and other geochemical proxy records. Seawater $^{87}Sr/^{86}Sr$-based estimates for this time-interval suggested a duration of ~1.694 Myr (McArthur et al., 2000), but this figure is problematic because of large-scale tectono-climatic events over this time-interval.

The radiometrically constrained age of 199.43 ± 0.10 Ma for the base-Sinemurian and the 183.8 ± 0.4 Ma age assigned here for the base-Toarcian stages, suggest a ~15.6 Myr duration for the combined Sinemurian and Pliensbachian stages (Schaltegger, 2008; Schoene, et al., 2010; Guex et al., 2012). In conjunction with the ~8.7 Myr duration of the Pliensbachian Stage estimated here, we suggest that the Sinemurian stage was ~700 kyr shorter than previously estimated and had a duration of 6.9 ± 0.4 Myr, with a 192.5 ± 0.4 Ma age for the base-Pliensbachian (the ± 0.4 Ma uncertainty derives from the combined radiometric and astrochronological uncertainty on the age of Lower Toarcian ash-beds in Peru and the duration of the Early Toarcian *tenuicostatum* zone, respectively) (Figure 6; Table 1).

An astronomically calibrated absolute time-scale has been constructed successfully for the Neogene and part of the Paleogene (Hilgen et al., 2014). Astronomical solutions for the geological past, however, become increasingly unpredictable, especially before ~50 Ma, due to multiple secular resonances in the inner solar system, and in particular with respect to the θ argument ($\theta = (s_4 - s_3) - 2(g_4 - g_3)$, where g_3 and g_4 are related to precession of the perihelion and s_3 and s_4 are related to precession of the node of Earth and Mars) (Laskar et al., 2004; Laskar et al., 2011). The 405 kyr eccentricity cycle, related to the ($g_2 - g_5$) argument, which reflects the motions of the orbital perihelia of (gravitational pull between) Jupiter and Venus, however, remained relatively stable over the past 250 million years (Laskar et al., 2004). Different solutions for the 405-kyr periodicity show a maximum deviation of 2π over 250 Myr, corresponding to a maximum error of <350 kyr at 200 Ma (Laskar et al., 2004; Laskar et al., 2011). The 405 kyr eccentricity solution, combined with precise radiometric anchor points, can therefore be used as a target curve for the astronomical tuning of floating astronomical time scales, potentially even back into the Mesozoic.

Precise radiometric and astrochronological age constraints for the base of the Hettangian and the base of the Sinemurian potentially allow the Hettangian floating astronomical time-scales to be accurately anchored to the stable 405 kyr eccentricity solution (La2010d) of Laskar et al. (2011) (Figure 6). However, given the radiometric and astrochronological uncertainties for the age of the base-Toarcian (and with that the age of the base-Pliensbachian), we are presently unable to confidently anchor the Pliensbachian floating astronomical time-scale obtained here to the absolute time scale and 405 kyr astronomical solution of Laskar et al. (2011). We therefore propose 3 different models, Options A, B and C (Figure 6). Option-A represents the solution with the youngest base Jurassic and oldest base Toarcian, Option-B represents the solution with the oldest base Jurassic and youngest base Toarcian, and Option-C represents the intermediate case (Figure 6). Importantly, different solutions for the 405 kyr periodicity, show a maximum deviation of <350 kyr in the Early Jurassic (Laskar et al., 2004), which adds additional uncertainty to this tuning. Consequently, it is currently not possible to assign with confidence particular observed peaks in the proxy records to either the maxima or minima of the 405 kyr eccentricity cycle.

[5.6] RATE AND DURATION OF PLIENSBACHIAN CLIMATIC AND GLOBAL CARBON-CYCLE CHANGE

The Early Jurassic was marked by large perturbations in global geochemical cycles, palaeoclimate and the palaeoenvironment, especially at the Triassic–Jurassic transition and in the Early Toarcian (Hesselbo et al., 2002; Jenkyns, 2003, 2010; Korte et al., 2009; Korte and Hesselbo, 2011; Ruhl et al., 2011; Suan et al., 2011; Ullmann et al., 2014; Brazier et al., 2015; Krencker et al., 2015; Al-Suwaidi et al., *in press*; and many others).

Recent studies show that the Pliensbachian stage was also marked by major perturbations in the global carbon cycle and possibly (global) climate. The Early Pliensbachian *jamesoni* zone is marked by a negative shift in $\delta^{13}C$ (of 2–4‰) in marine calcite and organic matter (Jenkyns et al., 2002; van de Schootbrugge et al., 2005; Woodfine et al., 2008; Korte and Hesselbo, 2011; Armendariz et al., 2012; Franceschi et al, 2014; Korte et al., 2015). This shift is also seen in the $\delta^{13}C$ of wood, reflecting global atmospheric change and a rearrangement of the global exogenic carbon cycle, possibly by the release of isotopically depleted carbon into the ocean-atmosphere system (Korte and Hesselbo, 2011). The late Pliensbachian *margaritatus* zone (*subnodosus-gibbosus* subzones) is further marked by a distinct positive shift in $\delta^{13}C$ of marine and terrestrial organic matter, marine calcite and wood (Jenkyns and Clayton, 1986; van de Schootbrugge et al., 2005; Suan et al., 2010; Korte and Hesselbo, 2011; Silva et al., 2011), possibly linked to enhanced carbon burial, under favourable marine redox conditions (Hesselbo and Jenkyns, 1995; Suan et al., 2010; Korte and Hesselbo, 2011; Silva et al., 2011; Silva and Duarte, 2015). Possible changes in Pliensbachian atmospheric pCO_2 may have affected regional and/or global temperatures (Suan et al., 2008; Suan et al., 2010; Korte and Hesselbo, 2011; Armendariz et al., 2013; Steinthorsdottir and Vajda, 2013; Silva and Duarte, 2015).

The tuned astrochronological Pliensbachian time scale presented here suggests that the Early Pliensbachian negative CIE had a duration of ~2 Myr, possibly linked to a recurrent phase of CAMP magmatism (see also section 5.7; Figure 7 and 8). The late Pliensbachian (late *margaritatus*) $\delta^{13}C$ positive excursion may have been marked by significant sea-level fluctuations and periodic sea-level low-stand, possibly in synchronicity with decreased shallow-marine benthic temperatures (Hesselbo et al., 2008; Korte and Hesselbo, 2011). The late Pliensbachian (late *margaritatus* zone) positive excursion has an estimated duration of ~0.6 Myr (Figure 7).

[5.7] CAMP VOLCANISM AND THE EARLY JURASSIC STEPPED $^{87}Sr/^{86}Sr$ RECORD

Seawater $^{87}Sr/^{86}Sr$ ratios and strontium (Sr) fluxes to the oceans are controlled by hydrothermal circulation at mid-ocean ridges and other types of basalt-seawater interaction, the continental weathering of silicates, and the dissolution of carbonates, while the fluxes out of the ocean are primarily regulated by carbonate burial (Burke et al., 1982; Elderfield, 1986; Steuber and Veizer, 2002; Krabbenhöft et al., 2010; Ullmann et al., 2013). Changes in seawater $^{87}Sr/^{86}Sr$ ratios can therefore be explained by the change in the relative importance of weathering (or a change in the Sr-isotopic composition of the weathering flux) and hydrothermal inputs of Sr into the oceans. The global unradiogenic strontium flux from hydrothermal venting and fresh ocean-crust weathering along mid-ocean ridges and by weathering of island arc basalts, is likely relatively stable over shorter time scales, but may have varied on tectonic time scales, with changes in the rate of ocean-crust formation along mid-ocean ridge systems and changes in the global extent of spreading ridges and ocean island arcs (Allègre et al., 2010; Van der Meer et al., 2014). The global unradiogenic Sr-flux may also have varied on long (> million year) Milankovitch periodicities, possibly in response to eustatic sea-level change and changing mid-ocean ridge spreading rates (Cohen and Coe, 2007; Crowley et al., 2015).

In the Early Jurassic, seawater $^{87}Sr/^{86}Sr$ ratios show an overall decrease over ~20 Myr towards unradiogenic values, from ~0.70775 to ~0.70705 (Jones et al., 1994; Cohen and Coe, 2007). Proto-Atlantic rifting at this time initiated on the continents, but continued throughout the Jurassic as mid-ocean ridge activity. Increased mid-ocean ridge spreading rates and/or the increased global extent of mid-ocean spreading ridges, combined with the possible increased formation of island arcs, may have provided an enhanced unradiogenic strontium flux to the global oceans (Van der Meer et al., 2014), leading to the observed steady decrease in Early Jurassic seawater $^{87}Sr/^{86}Sr$ until the Pliensbachian-Toarcian boundary (Jones et al., 1994; Jenkyns et al., 2002). A decline in seawater $^{87}Sr/^{86}Sr$ may alternatively be explained by a decrease in the overall continental weathering flux. However, in the absence of a major orogeny in the Early and Middle Jurassic, the $^{87}Sr/^{86}Sr$ ratio of the global weathering flux probably remained relatively stable (Jones et al., 1994). The changing style of biomineralization shown by the evolutionary adoption of calcite in Jurassic calcifying organisms, and increasing pelagic calcite production, likely did not play a major role in the observed change in seawater chemistry because seawater Sr/Ca ratios changed in parallel with Sr-isotope ratios, indicating a likely common weathering and/or tectonic origin for both (Ullmann et al., 2013).

The base Jurassic Hettangian stage, however, contrasts in being marked by a ~2 Myr 'plateau', with stable $^{87}Sr/^{86}Sr$ ratios of ~0.70775 (Cohen and Coe, 2007), suggesting the balancing of the unradiogenic Sr flux from basalt-seawater interaction, by the supply of radiogenic Sr from the weathering of old continental crust. This period was also marked by major flood-basalt emplacement, with the onset of CAMP volcanism in the latest Triassic, time-equivalent with the end-Triassic mass extinction, at ~201.4 Ma. Its onset preceded the Triassic–Jurassic boundary, defined by the first occurrence of the Jurassic ammonite species *Psiloceras spelae tirolicum*, by 100–200 kyr (Marzoli et al., 1999; Hesselbo et al., 2002; Deenen et al., 2010, 2011; Ruhl et al., 2010; Schoene et al., 2010; Whiteside et al., 2010; Ruhl and Kürschner, 2011; Blackburn et al., 2013; von Hillebrandt et al., 2013; Dal Corso et al., 2014; Hüsing et al., 2014). Astrochronological and radiometric dating constrain emplacement of the major CAMP flood-basalt pulses in the eastern North American Newark, Culpeper, Hartford and Deerfield Basins, the Canadian Fundy Basin, the Algarve in Portugal, the Moroccan Argana Basin and the Moroccan High Atlas Mountains, within a relatively short period of time, possibly within 1 million years after its onset (Olsen et al., 2003; Deenen et al., 2010, 2011; Marzoli et al., 2011; Fernandes et al., 2014). The chemical weathering of juvenile basaltic rocks from CAMP is, however, unlikely to have been directly responsible for stabilizing the Hettangian seawater $^{87}Sr/^{86}Sr$ signal, because Sr-isotope values of fresh Large Igneous Province basalts (with values of 0.704–0.706), are much less radiogenic than ambient Early Jurassic seawater (Cohen and Coe, 2007).

The release of volcanogenic CO_2 and biogenic and thermogenic methane from sea-floor clathrates and subsurface organic-rich facies following CAMP flood-basalt emplacement and dyke and sill intrusions (Hesselbo et al., 2002; Korte et al. 2009; Ruhl et al., 2011;

Schaller et al., 2011), combined with enhanced greenhouse-gas-induced elevated hydrological cycling (Ruhl et al., 2011; Bonis and Kürschner, 2012), may have enhanced the global weathering of crustal silicates, carbonates and evaporites and the subsequent flux of more radiogenic Sr to the global oceans (Jones and Jenkyns, 2001; Cohen and Coe, 2007).

CAMP-attributed flood-basalt emplacement and dyke and sill intrusions may, however, have continued for millions of years into the Early Jurassic, with a late phase of CAMP magmatism dated as of Early–Middle Pliensbachian age by $^{40}Ar/^{39}Ar$ (Baksi and Archibald, 1997; Deckart et al., 1997; Marzoli et al., 1999; Hames et al., 2000; Marzoli et al., 2004; Knight et al., 2004; Beutel et al., 2005; Verati et al., 2007; Nomade et al., 2007; Jourdan et al., 2009; Marzoli et al., 2011).

Sinemurian and Pliensbachian seawater $^{87}Sr/^{86}Sr$ ratios are often considered to show a relatively constant decline towards the Early Toarcian minimum (with values down to ~0.70705), at which point in time relatively enhanced continental silicate weathering in response to Early Toarcian Karoo-Ferrar volcanism induced a rapid reversal of this trend to renewed relatively elevated seawater $^{87}Sr/^{86}Sr$ values (Cohen and Coe, 2007). However, this observed constant rate of decline in seawater $^{87}Sr/^{86}Sr$ may be an artefact of the assumption of equal duration ammonite (sub-)zones. Conversion of the Pliensbachian seawater $^{87}Sr/^{86}Sr$ record of Jones et al. (1994) and Jenkyns et al. (2002) to the Pliensbachian astrochronological time-scale proposed here shows 4 distinct phases of enhanced decline in seawater $^{87}Sr/^{86}Sr$ superimposed on the Early Jurassic long-term decline and with a potential periodicity of ~2.4 Myr (Figure 8). The veracity of the observed changes in this trend relies on the accuracy of the positioning of the base of individual ammonite (sub)zones in both the outcrops and especially the Mochras core, and their precision as time-markers. Although ammonite stratigraphy in drill-cores might generally be less precise compared to that in outcrops, where fossil occurrences can be traced along extended bedding-planes, the precision of the assigned bases of (sub)zones in the Mochras core was further refined by the identification and correlation of recognized foraminiferal zones (Copestake and Johnson, 2013). The phases of enhanced decline in seawater $^{87}Sr/^{86}Sr$ may reflect periodic, long-term (> million year) Milankovitch-forced, decreases in global continental weathering rates, with a diminished flux of radiogenic Sr. Interestingly, the onset of the Pliensbachian stage is also marked by a plateau in seawater $^{87}Sr/^{86}Sr$ ratios, with stable values for ~2 Myr, closely resembling the pattern in the base Jurassic Hettangian Stage during the major phase of CAMP emplacement (Figure 8). This plateau in $^{87}Sr/^{86}Sr$ temporally coincides with a late phase of CAMP magmatism, with surface flood-basalt and subsurface sill emplacement in the eastern USA, Brazil and Guinea (Figure 8; Deckart et al., 1997; Marzoli et al., 1999; Nomade et al., 2007). The onset and duration of this plateau in $^{87}Sr/^{86}Sr$ also directly coincides with the earliest Pliensbachian (*jamesoni* zone) negative CIE, similar in magnitude (~2–4‰) and duration to the earliest Jurassic (Hettangian stage) long-term 'main' negative CIE (Figure 8; Hesselbo et al., 2002; Korte et al., 2009; Ruhl et al., 2010; Bartolini et al. 2012). The observed Early Pliensbachian plateau in $^{87}Sr/^{86}Sr$ ratios may, therefore, reflect a second Early Jurassic phase of CAMP-induced climatic and carbon-cycle perturbation that, as inferred for the Hettangian, also led to increased global weathering and an enhanced radiogenic Sr flux from the continents to the oceans. The inference of the Early Pliensbachian plateau in $^{87}Sr/^{86}Sr$ ratios depends on (1) the correct biostratigraphical correlation between the $^{87}Sr/^{86}Sr$ record, as measured in outcrops, and the Mochras core-based Early Pliensbachian astrochronology and (2) the correctness of the interpreted unequal duration of Pliensbachian zones, specifically the Early Pliensbachian (*jamesoni*) (sub)zones. If the above is all correct, than one may conclude that subsequent phases of CAMP volcanism led to elevated atmospheric pCO_2 and increased global continental (silicate) weathering rates that balanced the dominant long-term unradiogenic marine hydrothermal/basalt weathering Sr flux and resulted in the observed (Hettangian and Early Pliensbachian) ~2 Myr plateaus in the Early Jurassic $^{87}Sr/^{86}Sr$ record.

[6] CONCLUSIONS

Periodic alternations in lithology and geochemical proxies in the Early Jurassic (Pliensbachian) through the expanded and biostratigraphically complete Mochras core (UK), reflect Milankovitch forcing, predominantly at precession and short- and long-eccentricity periodicities. The duration of Pliensbachian ammonite zones is cyclostratigraphically constrained at ~2.7 Myr (*jamesoni*), ~1.8 Myr (*ibex*), ~0.4 Myr (*davoei*), ~2.4 Myr (*margaritatus*) and ~1.4 Myr (*spinatum*), with a combined duration of ~8.7 Myr for the complete Pliensbachian Stage. These figures, combined with radiometric and astrochronological constraints on the age of the base of the Toarcian, suggests a Sinemurian–Pliensbachian boundary age of 192.5 ± 0.4 Ma.

Calibration of the obtained floating Pliensbachian astronomical timescale to the 405 kyr eccentricity solution (La2010d) gives absolute ages for the Pliensbachian ammonite zone boundaries and the base Pliensbachian (*jamesoni* zone) global exogenic carbon cycle perturbation. This latter 2–4‰ long-term negative excursion in $\delta^{13}C$ has an astrochronologically defined duration of ~2 Myr and is followed by the Upper Pliensbachian (Upper *margaritatus* zone) global positive excursion in $\delta^{13}C$, with a duration of ~0.6 Myr, and which coincides with a seawater cool phase in the European realm as revealed by $\delta^{18}O$ from macrofossil calcite.

Calibration of the Pliensbachian $^{87}Sr/^{86}Sr$ record to the obtained astrochronological time-series suggests modulation of the Pliensbachian long-term decreasing trend to less radiogenic values, with a ~2.4 Myr periodicity. The Pliensbachian $^{87}Sr/^{86}Sr$ record also shows a stable 'plateau' in the Early Pliensbachian *jamesoni* zone, coinciding with the observed $\delta^{13}C$ negative shift of 2–4‰, and possibly reflecting elevated continental weathering, with a relatively increased flux of radiogenic $^{87}Sr/^{86}Sr$ to the global oceans, in response to a late phase of enhanced global continental (silicate) weathering induced by CAMP volcanism.

ACKNOWLEDGEMENTS

MR, SPH, HCJ, WX, MS and DM acknowledge funding for this study from Shell International Exploration & Production B.V. We thank the British Geological Survey (BGS) for enabling access to the Mochras core and Charles J.B. Gowing (BGS) for supplying Hand-held XRF equipment and assistance with analyses. We also thank Steve Wyatt (Oxford) and Mabs Gilmour (Open University) for help with Rock-Eval and $\delta^{13}C$ analyses. JBR publishes with the approval of the Executive Director, British Geological Survey (NERC).

FIGURE CAPTIONS

FIGURE 1 Early Jurassic palaeogeography showing the Mochras (Cardigan Bay Basin) and Staithes (Cleveland Basin) localities (red stars) at the northwestern end of the Tethys Ocean. The figure is modified after Dera et al., 2011 and Korte et al., 2015.

FIGURE 2 The relative thickness of Lower Jurassic stages in the Mochras core and outcrops and boreholes in the UK, France and Portugal (Ivimey-Cook, 1971, 1982; Cope et al., 1980; Whittaker and Green, 1983; Lorenz and Gely, 1994; Ainsworth and Riley, 2010; Brigaud et al., 2014; Mattioli et al., 2013; and references therein). The 'T', 'HS' and 'PL' numbers refer to the stratigraphical columns in Cope et al. (1980).

FIGURE 3 Early Pliensbachian (*jamesoni* zone) lithology and XRF-derived geochemical data (calcium, titanium, iron, rubidium) showing sub-metre-scale fluctuations. Calcium concentrations are superimposed on stacked core-photos showing a clear association with lithology/rock-colour. Four to five carbonate beds group into bundles (E^{-1}) and super-bundles (E^{-2}), possibly representing short (~100 kyr) and long (~405 kyr) eccentricity. High values for Ti, Fe and Rb correlate closely with low concentrations of Ca, suggesting carbonate dilution.

FIGURE 4 XRF-derived calcium and titanium record spanning the full Pliensbachian Stage (from the Upper Sinemurian *raricostatum* zone into the Lower Toarcian *tenuicostatum* zone). Mochras-core biostratigraphy following Ivimey-Cook (1971), Page (2003), and Copestake and Johnson (2013). The palaeomagnetic field directions from numerous outcrop studies are correlated to the Mochras core biostratigraphical record following the Geological Time-Scale (GTS) 2012 (Gradstein et al., 2012). Ca content, superimposed on the stacked core-photos record, shows short-, intermediate- and long-periodicity fluctuations, with (A) the complete core, (B) part of the Upper Sinemurian *raricostatum* and complete Lower Pliensbachian *jamesoni* zones, (C) the Pliensbachian *ibex* and *davoei* zones and (D) the Upper Pliensbachian *margaritatus* and *spinatum* zones. The short- and intermediate-periodicity band-pass filters reflect dominant spectral peaks in the depth-domain (Supplementary Figure 2; see also section 5.3), suggesting a combined duration of ~8.7 Myr for the complete Pliensbachian stage (see Supplementary Figure 4). Grey arrows show intervals with possibly dominant obliquity forcing.

FIGURE 5 Multi-taper (MTM; 3π) spectral and wavelet analyses of the obtained XRF elemental (Fe) time series using the Astrochron toolkit (R (3.1.2) Package for astrochronology, version 0.3.1; Meyers, 2014), with robust red noise models (Mann and Lees, 1996). The elemental Fe record was first re-sampled to uniform sample spacing using linear interpolation. Initial spectral analysis was performed with AnalySeries on a detrended data-series (with low band-pass filtering to remove >150 m periodicities). Dominant spectral components (Supplementary Figure 2 and 3) were filtered from the data series and compared to the visually defined precession and short- and long-eccentricity periodicities (Figure 4). The elemental Fe record in the depth domain was subsequently converted to the time domain following the observed 405 kyr eccentricity cycles. The multi-taper (MTM; 3π) spectral and wavelet analyses of the obtained elemental (Fe) time series show dominant and significant peaks at precession (~21 and ~26 kyr), obliquity (~41 kyr), short-period eccentricity (~100 and ~134 kyr), long-period eccentricity (~405 kyr) and also long-term periodicity (~640 and 2500 kyr).

FIGURE 6 Calibration of the obtained Pliensbachian 405-kyr eccentricity series to the astronomical solution (La2010d) of Laskar et al. (2011) allows for 3 different options (A, B and C) due to the ~250 kyr uncertainty in U-Pb radiometric dating of the base *falciferum* zone in the Pucara Basin (Peru) and the ~200 kyr uncertainty in the astrochronologically estimated duration of the base Toarcian *polymorphum* (*tenuicostatum*) zone in the Lusitanian Basin (Portugal) (see also section 7.2). Radiometric and astrochronological constraints on the age of the base-Hettangian (Triassic-Jurassic) and base-Sinemurian stage boundaries and the duration of the Hettangian stage and the *polymorphum* zone come from Kent and Olsen (2008), Schaltegger et al. (2008), Suan et al. (2008), Ruhl et al. (2010), Schoene et al. (2010), Guex et al. (2012), Blackburn et al. (2013), Huang and Hesselbo (2014), Hüsing et al. (2014) and Sell et al. (2014). Orange bars present the reported radiometric uncertainty. The Hettangian palaeomagnetic record comes from Kent and Olsen (2008) and Hüsing et al. (2014). The Pliensbachian palaeomagnetic record comes from the Geological Time-Scale (GTS) 2012 (Gradstein et al., 2012).

FIGURE 7 The Pliensbachian $\delta^{13}C$ record of marine calcite and wood from UK outcrops (Jenkyns et al., 2002; Korte and Hesselbo, 2011) and $\delta^{13}C$ of bulk organic matter ($\delta^{13}C_{TOC}$) from Staithes (this study; Yorkshire, UK (locality described in Korte and Hesselbo, 2011), calibrated to the Pliensbachian floating astronomical time-scale, using zone boundaries as tie-points and linear-interpolation within a zone.

FIGURE 8 The Pliensbachian seawater $^{87}Sr/^{86}Sr$ record calibrated against the here obtained floating astrochronological time scale, using subzone boundaries in outcrops (that yielded $^{87}Sr/^{86}Sr$ data) and the Mochras core as tie-points, and linear interpolation within ammonite subzones. The time-calibrated $^{87}Sr/^{86}Sr$ record shows periodically enhanced decline (grey arrows) superimposed on a long-term decrease from ~0.70745 to ~0.70710. The base of the Pliensbachian is, furthermore, marked by a 'plateau' in $^{87}Sr/^{86}Sr$ (blue arrows), coinciding with a global carbon cycle perturbation and recurrent Central Atlantic Magmatic Province (CAMP) volcanism. Lower Jurassic $^{87}Sr/^{86}Sr$ values are from Jones et al. (1994) and Jenkyns et al. (2002) (data was normalized to a value of the NBS987 standard of 0.710250, with $24*10^{-6}$ added to the published data of Jones et al. (1994), which was normalized to a different standard). The Pliensbachian $\delta^{13}C$ record is from Jenkyns et al. (2002) and Korte and Hesselbo (2011). Upper Triassic/Lower Jurassic radiometric dating of CAMP magmatism comes from Baksi and Archibald (1997), Deckart et al. (1997), Marzoli et al. (1999), Hames et al. (2000), Marzoli et al. (2004), Knight et al. (2004), Beutel et al. (2005), Verati et al. (2007), Nomade et al. (2007), Jourdan et al. (2009), Marzoli et al. (2011) and Blackburn et al. (2013). The dark grey area in the upper graph shows the cumulative probability of CAMP magmatism through time, following uncertainties on $^{40}Ar/^{39}Ar$ and U-Pb radiometric dating of individual basalt formations.

TABLE 1 Absolute age and duration estimates for the base of the Early Jurassic stages (Hettangian, Sinumurian, Pliensbachian and Toarcian) and the Hettangian and Pliensbachian zones. Basal-age and durations based on Kent and Olsen (2008), Schaltegger et al. (2008), Suan et al. (2008), Ruhl et al. (2010), Schoene et al. (2010), Guex et al. (2012), Blackburn et al. (2013), Boulila et al., 2014; Huang and Hesselbo (2014), Hüsing et al. (2014), Ruebsam et al., 2014 and Sell et al. (2014).

REFERENCES

Allègre, C.J., Louvat, P., Gaillardet, J., Meynadier, L., Rad, S., Capmas, F., the fundamental role of island arc weathering in the oceanic Sr isotope budget. Earth and Planetary Science Letters 292, p. 51–56 (2010).

Al-Suwaidi, A.H., Hesselbo, S.P., Damborenea, S.E., Mancenido, M.O., Jenkyns, H.C., Riccardi, A.C., Angelozzi, G.N., Baudin, F., The Toarcian Oceanic Anoxic Event (Early Jurassic) in the Neuquén Basin, Argentina: a reassessment of age and carbon-isotope stratigraphy. The Journal of Geology, *in press*.

Armendariz, M., Rosales, I., Badenas, B., Aurell, M., Garcia-Ramos, J.C., Pinuela, L., High-resolution chemostratigraphic records from the Lower lPliensbachian belemnites: Palaeoclimatic perturbations, organi facies and water mass exchange (Asturian basin, northern Spain). Palaeogeography, Palaeoclimatology, Palaeoecology 333-334, p. 178–191 (2012).

Armendariz, M., Rosales, I., Badenas, B., Pinuela, L., Aurell, M., Garcia-Ramos, J.C., An approach to estimate Lower Jurassic seawater oxygen-isotope composition using $\delta^{18}O$ and Mg/Ca ratios of belemnite calcites (Early Pliensbachian, northern Spain). Terra Nova 25, p. 439–445 (2013).

Baksi, A.K., Archibald, D.A., Mesozoic igneous activity in the Maranhao province, northern Brazil: $^{40}Ar/^{39}Ar$ evidence for separate episodes of basaltic magmatism. Earth and Planetary Science Letters 151, p. 139–153 (1997).

Bartolini, A., Guex, J., Spangenberg, J.E., Schoene, B., Taylor, D.G., Schaltegger, U., Atudorei, V., Disentangling the Hettangian carbon isotope record: Implications for the aftermath of the end-Triassic mass extinction. Geochemistry, Geophysics, Geosystems 13, no. 1 (2012).

Beutel, E.K., Nomade, S., Fronabarger, A.K., Renne, P.R., Pangea's complex breakup: A new rapidly changing stress field model. Earth and Planetary Science Letters 236, p. 471–485 (2005).

Blackburn, T.J., Olsen, P.E., Bowring, S.A., McLean, N.M., Kent, D.V., Puffer, J., McHone, G., Rasbury, E.T., Et-Touhami, M., Zircon U-Pb geochronology links the end-triassic extinction with the Central Atlantic Magmatic Province. Science 340, p. 941–945 (2013).

Bonis, N.R., Kurschner, W.M., Vegetation history, diversity patterns, and climate change across the Triassic/Jurassic boundary. Paleobiology 38, no. 2, p. 240–264 (2012).

Boulila, S., Galbrun, B., Huret, E., Hinnov, L.A., Rouget, I., Gardin, S., Huang, C., and Bartolini, A. (2014), Astronomical calibration of the Toarcian Stage: implications for sequence stratigraphy and duration of the Early Toarcian OAE, Earth and Planetary Science Letters, 386, 98-111.

Brazier, J.-M., Suan, G., Tacail, T., Simon, L., Martin, J.E., Mattioli, E., Balter, V., Calcium isotopic evidence for dramatic increase of continental weathering during the Toarcian oceanic anoxic event (Early Jurassic). Earth and Planetary Science Letters 411, p. 164–176 (2015).

Burgess, S.D., Bowring, S.A., Fleming, T.H., Elliot, D.H., High-precision geochronology links the Ferrar large igneous province with Early Jurassic ocean anoxia and biotic crisis. Earth and Planetary Science Letters 415, P. 90–99 (2015).

Burke, W.H., Denison, R.E., Hetherington, E.A., Koepnick, R.B., Nelson, H.F., Otto, J.B., Variation of seawater $^{87}Sr/^{86}Sr$ throughout Phanerozoic time. Geology 10, p. 516–519

(1982).

Clemence, M.-E., Bartolini, A., Gardin, S., Paris, G., Beaumont, V., Page, K.N., Early Hettangian benthic-planktonic coupling at Doniford (SW England) Palaeoenvironmental implications for the aftermath of the end-Triassic crisis. Palaeogeography, Palaeoclimatology, Palaeoecology 295, p. 102–115 (2010).

Close, R.A., Friedman, M., Lloyd, G.T., Benson, R.B.J., Evidence for a Mid-Jurassic Adaptive Radiation in Mammals. Current Biology 25, p. 1–6 (2015).

Cohen, A.S., Coe, A.L., Harding, S.M., Schwark, L., Osmium isotope evidence for the regulation of atmospheric CO_2 by continental weathering. Geology 32, n. 2, p. 157–160 (2004).

Cohen, A.S., Coe, A.L., The impact of the Central Atlantic Magmatic Province on climate and on the Sr- and Os-isotope evolution of seawater. Palaeogeography, Palaeoclimatology, Palaeoecology 244, p. 374–390 (2007).

Copestake, P., Johnson, B., Lower Jurassic foraminifera from the Llanbedr (Mochras Farm) borehole, North Wales, UK. Monograph of the Palaeontographical Society, London 167, p. 1–403 (2013).

Crowley, J.W., Katz, R.F., Huybers, P., Langmuir, C.H., Park, S.-H., Glacial cycles drive variations in the production of oceanic crust. Science 347, p. 1237–1240 (2015).

Dal Corso, J., Marzoli, A., Tateo, F., Jenkyns, H.C., Bertrand, H., Youbi, N., Mahmoudi, A., Font, E., Buratti, N., Cirilli, S., The dawn of CAMP volcanism and its bearing on the end-Triassic carbon cycle disruption. Journal of the Geological Society, London 171, p. 153–164 (2014).

Deckart, K., Feraud, G., Bertrand, H., Age of Jurassic continental tholeiites of French Guyana, Surinam and Guinea: Implications for the initial opening of the Central Atlantic Ocean. Earth and Planetary Science Letters 150, p. 205–220 (1997).

Deenen, M.H.L., Krijgsman, W., Ruhl, M., The quest for chron E23r at Partridge Island, Bay of Fundy, Canada: CAMP emplacement postdates the end-Triassic extinction event at the North American craton. Can. J. Earth Sci. 48, p. 1282–1291 (2011).

Deenen, M.H.L., Ruhl, M., Bonis, N.R., Krijgsman, W., Kuerschner, W.M., Reitsma, M., van Bergen, M.J., A new chronology for the end-Triassic mass extinction. Earth and Planetary Science Letters 291, p. 113–125 (2010).

Dera, G., Neige, P., Dommergues, J.-L., Brayard, A., Ammonite paleobiogeography during the Pliensbachian–Toarcian crisis (Early Jurassic) reflecting paleoclimate, eustasy, and extinctions. Global and Planetary Change 78, p. 92–105 (2011).

Dobson M.R., Whittington, R.J., The geology of Cardigan Bay, Proceedings of the Geologists' Association 98, p. 331–353 (1987).

Elderfield, H., Strontium isotope stratigraphy, Palaeogeography, Palaeoclimatology, Palaeoecology 57, p. 71–90 (1986).

Fernandes, S., Font, E., Neres, M., Martins, L., Youbi, N., Madeira, J., Marzoli, A., The Central Atlantic Magmatic Province (CAMP) in Portugal, high eruption rate in one short-lived volcanic pulse. Comunicacoes Geologicas 101, p. 1449–1453 (2014).

Franceschi, M., Dal Corso, J., Posenato, R., Roghi, G., Masetti, D., Jenkyns, H.C., Early Pliensbachian (Early Jurassic) C-isotope perturbation and the diffusion of the Lithiotis Fauna: Insights from the western Tethys. Palaeogeography, Palaeoclimatology, Palaeoecology 410, p. 255–263 (2014).

Gomez, J.J., Comas-Rengifo, M.J., Goy, A., Palaeoclimatic oscillations in the Pliensbachian (Lower Jurassic) of the Asturian Basin (Northern Spain). Clim. Past Discuss. 11, p. 4039–4076 (2015).

Gradstein, F.M., Ogg, J.G., Schmitz, M.D., Ogg, G.M., The Geological Time Scale 2012, Volume 1 & 2, Elsevier, ISBN: 978-0-44-459390-0 & 978-0-44-459434-1 (2012).

Guex, J., Bartolini, A., Spangenberg, J., Vicente, J.-C., Schaltegger, U., Ammonoid multi-extinction crises during the Late Pliensbachian–Toarcian and carbon cycle instabilities. Solid Earth Discussions 4, p. 1205–1228 (2012).

Guex, J., Schoene, B., Bartolini, A., Spangenberg, J., Schaltegger, U., O'Dogherty, L., Taylor, D., Bucher, H., Atudorei, V., Geochronological constraints on post-extinction recovery of the ammonoids and carbon cycle perturbations during the Early Jurassic. Palaeogeography, Palaoeclimatology, Palaeoecology 346-347, p. 1–11 (2012).

Hallam, A., Esitmates of the amount and rate of sea-level change across the Rhaetian-Hettangian and Pliensbachian-Toarcian boundaries (latest Triassic to Early Jurassic). Journal of the Geological Society 154, p. 773–779 (1997).

Hallam, A., Origin of minor limestone-shale cycles: Climatically induced or diagenetic? Geology 14, p. 609–612 (1986).

Hames, W.E., Renne, P.R., Ruppel, C., New evidence for geological instantaneous emplacement of earliest Jurassic central Atlantic Magmatic Province basalts on the North American margin. Geology 28, no. 9, p. 859–862 (2000).

Hesselbo, S.P., Bjerrum, C.J., Hinnov, L.A., MacNiocaill, C., Miller, K.G., Riding, J.B., van de Schootbrugge, B., and the Mochras Revisited Science Team, Mochras borehole revisited: a new global standard for Early Jurassic earth history. Sci. Dril. 16, p. 81–91 (2013).

Hesselbo, S.P., Jenkyns, H.C., A comparison of the Hettangian to Bajocian successions of Dorset and Yorkshire. From Taylor, P.D. (Ed.): Field Geology of the British Jurassic. Geological Society, London, p. 105–150 (1995).

Hesselbo, S.P., Meister, C., Grocke, D.R., A potential global stratotype for the Sinemurian-Pleinsbachian boundary (Lower Jurassic), Robin Hood's Bay, UK: ammonite faunas and isotope stratigraphy. Geological Magazine 137, p. 601–607 (2000).

Hesselbo, S.P., Robinson, S.A., Surlyk, F., Piasecki, S., Terrestrial and marine extinction at the Triassic-Jurassic boundary synchronized with major carbon-cycle perturbation: A link to initiation of massive volcanism? Geology 30, no. 3, p. 251–254 (2002).

Hesselbo, S.P., Robinson, S.A., Surlyk, F., Sea-level change and facies development across potential Triassic-Jurassic boundary horizons, SW Britain. Journal of the Geological Society, London 161, p. 365–379 (2004).

Hesselbo, S.P., Sequence stratigraphy and inferred relative sea-level change from the onshore British Jurassic. Proceedings of the Geologists' Association 119, p. 19–34 (2008).

Hilgen, F.J., Hinnov, L.A., Abdul Aziz, H., Abels, H.A., Batenburg, S., Bosmans, J.H.C., de Boer, B., Hüsing, S.K., Kuiper, K.F., Lourens, L.J., Rivera, T., Tuenter, E., Van de Wal, R.S.W., Wotzlaw, J.-F., Zeeden, C., Stratigraphic continuity and fragmentary sedimentation: the success of cyclostratigraphy as part of integrated stratigraphy. From: Smith, D.G., Bailey, R.J., Burgess, P.M., Fraser, A.J. (eds): Strata and Time: Probing the gaps in our understanding. Geological Society, London, Special Publication 404 (2014).

Huang, C., Hesselbo, S.P., Pacing of the Toarcian Oceanic Anoxic Event (Early Jurassic) from astronomical correlation of marine sections. Gondwana Research 25, p. 1348–1356 (2014).

Hüsing, S.K., Beniest, A., Van der Boon, A., Abels, H.A., Deenen, M.H.L., Ruhl, M., Krijgsman, W., Astronomically-calibrated magnetostratigraphy of the Lower Jurassic marine successions at St' Audrie's Bay and East Quantoxhead (Hettangian-Sinemurian; Somerset, UK). Palaeogeography, Palaoeclimatology, Palaeoecology 403, p. 43–56 (2014).

Ivimey-Cook, H.C., Stratigraphical Palaeontology of the Lower Jurassic of the Llanbedr (Mochras Farm) Borehole. In: Woodland, A.W. (Ed). The Llanbedr (Mochras Farm) Borehole. Institute of Geological Sciences Report No. 71/18, p. 87–92 (1971).

Jenkyns, H.C., Clayton, C.J., Black shales and carbon isotopes in pelagic sediments from the Tethyan Lower Jurassic. Sedimentology 33, p. 87–106 (1986).

Jenkyns, H.C., Evidenc for rapid climate change in the Mesozoic–Palaeogene greenhouse world. Phil. Trans. R. Soc. London. A 361, p. 1885-1916 (2003).

Jenkyns, H.C., Geochemistry of oceanic anoxic events. Geochemistry, Geophysics, Geosystems 11, no. 3, Q03004, DOI: 10.1029/2009GC002788 (2010).

Jenkyns, H.C., Jones, C.E., Grocke, D.R., Hesselbo, S.P., Parkinson, D.N., Chemostratigraphic of the Jurassic System: applications, limitations and implications for palaeoceanography. Journal of the Geological Society 159, p. 351–378 (2002).

Jenkyns, H.C., Weedon, G.P., Chemostratigraphic ($CaCO_3$, TOC, $\delta^{13}C_{org}$) of Sinemurian (Lower Jurassic) black shales from the Wessex Basin, Dorset and palaeoenvironmental implications. Newsletters on Stratigraphy 46, no. 1, p. 1–21 (2013).

Jones, C.E., Jenkyns, H.C., Hesselbo, S.P., Strontium isotopes in Early Jurassic seawater. Geochimica et Cosmochimica Acta 58, no. 4, p. 1285–1301 (1994).

Jones, C.E., Jenkyns, H.C., Seawater strontium isotopes, oceanic anoxic events, and seafloor hydrothermal activity in the Jurassic and Cretaceous. American Journal of Science 301, p. 112–149 (2001).

Jourdan, F., Marzoli, A., Bertrand, H., Cirilli, S., Tanner, L.H., Kontak, D.J., McHone, G., renne, P.R., Bellieni, G., ^{40}Ar/^{39}Ar age of CAMP in North America: Implications for the Triassic-Jurassic boundary and the ^{40}K decay constant bias. Lithos 110, p. 167–180 (2009).

Kemp, D.B., Coe, A.L., Cohen, A.S., Weedon, G.P., Astronomical forcing and chronology of the Early Toarcian (Early Jurassic) oceanic anoxic event in Yorkshire, UK. Paleoceanography 26, PA4210 (2011).

Kent, D.V., Olsen, P.E., Early Jurassic magnetostratigraphy and paleolatitudes from the Hartford continental rift basin (eastern North America): Testing for polarity bias and abrupt polar wander in association with the Central Atlantic Magmatic Province. J. Geophys. Res. 113 (2008).

Knight, K.B., Nomade, S., Renne, P.R., Marzoli, A., Bertrand, H., Youbi, N., The Central Atlantic Magmatic Province at the Triassic-Jurassic boundary: paleomagnetic and ^{40}Ar/^{39}Ar evidence from Morocco for brief, episodic volcanism. Earth and Planetary Science Letters 228, p. 143–160 (2004).

Korte, C., Hesselbo, S.P., Jenkyns, H.C., Rickaby, R.E.M., Spotl, C., Palaeoenvironmental significance of carbon- and oxygen-isotope stratigraphy of marine Triassic Jurassic boundary sections in SW Britain. Journal of the Geological Society 166, p. 431–445 (2009).

Korte, C., Hesselbo, S.P., Shallow marine carbon and oxygen isotopic and elemental records indicate icehouse-greenhouse cycles during the Early Jurassic. Paleoceanography 26, PA4219 (2011).

Korte, C., Hesselbo, S.P., Ullmann, C.V., Dietl, G., Ruhl, M., Schweigert, G., Thibault, T., Jurassic climate mode governed by ocean gateway. Nat. Commun. 6, p. 10015 (2015).

Krabbenhoft, A., Eisenhauer, A., Bohm, F., Vollstaedt, H., Fietzke, J., Liebetrau, V., Augustin, N., Peucker-Ehrenbrink, B., Muller, M.N., Horn, C., Hansen, B.T., Nolte, N., Wallmann, K., Constraining the marine strontium budget with natural strontium isotope fractionations ($^{87}Sr/^{86}Sr^*$, $\delta^{88/86}Sr$) of carbonates, hydrothermal solutions and rivers. Geochimica et Cosmochimica Acta 74, p. 4097–4109 (2010).

Krencker, F.-N., Bodin, S., Suan, G., Heimhofer, U., Kabiri, L., Immenhauser, A., Toarcian extreme warmth led to tropical cyclone intensification. Earth and Planetary Science Letters 425, p. 120–130 (2015).

Laskar, J., Fienga, A., Gastineau, M., Manche, H., La2010: a new orbital solution for the long-term motion of the Earth. A & A 532, A89 (2011).

Laskar, J., Robutel, P., Joutel, F., Gastineau, M., Correia, A.C.M., Levrard, B., A long-term numerical solution for the insolation quantities of the Earth. A & A 428, p. 261–285 (2004).

Mann, M.E., Lees, J.M., Robust estimation of background noise and signal detection in climatic time series. Climatic Change 33, p. 409–445 (1996).

Marzoli, A., Bertrand, H., Knight, K.B., Cirilli, S., Buratti, N., Verati, C., Nomade, S., Renne, P.R., Youbi, N., Martini, R., Allenbach, K., Neuwerth, R., Rapaille, C., Zaninetti, L., Bellieni, G., Synchrony of the Central Atlantic Magmatic Province and the Triassic-Jurassic boundary climatic and biotic crisis. Geology 32, no. 11, p. 973–976 (2004).

Marzoli, A., Jourdan, F., Puffer, J.H., Cuppone, T., Tanner, L.H., Weems, R.E., Bertrand, H., Cirilli, S., Bellieni, G., De Min, A., Timing and duration of the Central Atlantic Magmatic Province in the Newark and Culpeper basins, eastern U.S.A. Lithos 122, p. 175–188 (2011).

Marzoli, A., Renne, P.R., Piccirillo, E.M., Ernesto, M., Bellieni, G., De Min, A., Extensive 200-million-year-old continental flood basalts of the Central Atlantic Magmatic Province. Science 284, p. 616 (1999).

McArthur, J.M., Donovan, D.T., Thirlwall, M.F., Fouke, B.W., Mattey, D., Strontium isotope profile of the Early Toarcian (Jurassic) oceanic anoxic event, the duration of ammonite biozones and belemnite palaeotemperatures. Earth and Planetary Science Letters 179, p. 269–285 (2000).

McElwain, J.C., Beerling, D.J., Woodward, F.I., Fossil Plants and Global Warming at the Triassic-Jurassic Boundary. Science 285, p. 1386 (1999).

Meister, C., Aberhan, M., Blau, J., Dommergues, J.-L., Feist-Burkhardt, S., Hailwood, E.A., Hart, M., Hesselbo, S.P., Hounslow, M.W., Hylton, M., Morton, N., Page, K., Price, G., the Global Boundary Stratotype Section and Point (GSSP) for the base of the Pleinsbachian Stage (Lower Jurassic), Wine haven, Yorkshire, UK. Episodes 20, no. 2, 93-106 (2006).

Meyers, S.R. (2014), Astrochron: An R Package for Astrochronology (Version 0.3.1). http://cran.r-project.org/package=astrochron

Morettini, E., Santantonio, M., Bartolini, A., Cecca, F., Baumgartner, P.O., Hunziker, J.C., Carbon isotope stratigraphy and carbonate production during the Early-Middle Jurassic: examples from the Umbria-Marche-Sabine Apennines (central Italy). Palaeogeograph, Palaeoclimatology, Palaeoecology 184, p. 251–273 (2002).

Nomade, S., Knight, K.B., Beutel, E., Renne, P.R., Verati, C., feraud, G., Marzoli, A., Youbi, N., Bertrand, H., Chronology of the Central Atlantic Magmatic Province: Implications for the Central Atlantic rifting process and the Triassic–Jurassic biotic crisis. Palaeogeography, Palaeoclimatology, Palaeoecology 244, p. 326–344 (2007).

Olsen, P.E., Kent, D.V., Et-Touhami, M., Puffer, J., Cyclo-, magneto, and bio-stratigraphic constraints on the duration of the CAMP event and its relationship to the Triassic-Jurassic boundary. From: The Central Atlantic Magmatic Province: Insights from fragments of Pangea. Geophysical Monograph 136, American Geophysical Union (2003).

Olsen, P.E., Stratigraphic record of the Early Mesozoic breakup of Pangea in the Laurasia-Gondwana rift system. Annu. Rev. Earth Planet. Sci. 25, p. 337–401 (1997).

Page, K.N., Bello, j., Dolores Lardies, M., Melendez, G., Ramajo, J., Ziani, H., The stratigraphy of the upper Bathonian to middle Oxfordian succession of the aragonese branch of the Cordillera Iberica (Spain) and its European context. Rivista Italiana do Paleontologia e Stratigrafia 110, no. 1, p. 191–200 (2004).

Page, K.N., The Lower Jurassic of Europe; its subdivision and correlation. Geological Survey of Denmark and Greenland Bulletin 1, p. 23–59 (2003).

Page, K.N., The Lower Jurassic of Europe: its subdivision and correlation. Geological Survey of Denmark and Greenland Bulletin 1, p. 23–59 (2003).

Paillard, D., L. Labeyrie and P. Yiou, Macintosh program performs time-series analysis, *Eos Trans. AGU,* 77: 379 (1996).

Pálfy, J., Smith, P.L., Synchrony between Early Jurassic extinction, oceanic anoxic event, and the Karoo-Ferrar flood basalt volcanism. Geology 28, n. 8, p. 747–750 (2000).

Porter S.J., Selby, D., Suzuki, K., Grocke, D., opening of a trans-Pangaean marine corridor during the Early Jurassic: Insights from osmium isotopes across the Sinemurian-Pliensbachian GSSP, Robin Hood's Bay, UK. Palaeogeography, Palaeoclimatology, Palaeoecology 375, p. 50–58 (2013).

Riding, J.B., Leng, M.J., Kender, S., Hesselbo, S.P., Feist-Burkhardt, S., Isotopic and palynological evidence for a new Early Jurassic environmental perturbation. Palaeogeography, Palaeoclimatology, Palaeoecology 374, p. 16-27 (2013).

Ruebsam, W., Munzberger, P., Schwark, L., Chronology of the Early Toarcian environmental crisis in the Lorraine Sub-Basin (NE Paris Basin). Earth and Planetary Science Letters 404, p. 273–282 (2014).

Ruebsam, W., Munzberger, P., Schwark, L., Reply to the comment by Boulila and Hinnov towards "Chronology of the Early Toarcian environmental crisis in the Lorraine Sub-Basin (NE Paris Basin). Earth and Planetary Science Letters 404, p. 273–282 (2014)". Earth and Planetary Science Letters 416, 147–150 (2015).

Ruhl, M., Bonis, N.R., Reichart, G.-J., Sinninghe Damste, J.S., Kürschner, W.M., Atmospheric carbon injection linked to End-Triassic mass extinction. Science 333, p. 430 (2011).

Ruhl, M., Deenen, M.H.L., Abels, H.A., Bonis, N.R., Krijgsman, W., Kürschner, W.M., Astronomical constraints on the duration of the Early Jurassic Hettangian stage and recovery rates following the end-Triassic mass extinction (St Audrie's Bay/ East Quantoxhead, UK). Earth and Planetary Science Letters 295, p. 262–276 (2010).

Ruhl, M., Kurschner, W.M., Multiple phases of carbon cycle disturbance from large igneous province formation at the Triassic-Jurassic transition. Geology 39, no. 5, p. 431–434 (2011).

Schaller, M. F., Wright, J.D., Kent, D.V., Atmospheric pCO2 perturbations associated with the Central Atlantic Magmatic Province. Science 331, p. 1404 (2011).

Schaltegger, U., Guex, J., Bartolini, A., Schoene, B., Ovtcharova, M., Precise U-Pb age constraints for end-Triassic mass extinction, its correlation to volcanism and Hettangian post-extinction recovery. Earth and Planetary Science Letters 267, p. 266–275 (2008).

Schoene, B., Guex, J., Bartolini, A., Schaltegger, U., Blackburn, T.J., Correlating the end-Triassic mass extinction and flood basalt volcanism at the 100 ka level. Geology 38, no. 5, p. 387–390 (2010).

Sell, B., Ovtcharova, M., Guex, J., Bartolini, A., Jourdan, F., Spangenberg, J.E., Vicente, J.-C., Schaltegger, U., Evaluating the temporal link between the Karoo LIP and climatic-biologic events of the Toarcian Stage with high-precision U-Pb geochronology. Earth and Planetary Science Letters 408, p. 48–56 (2014).

Sellwood, B.W., Regional environmental changes across a Lower Jurassic stage-boundary in Britain. Palaeontology 15, no. 1, p. 125 (1972).

Sellwood, B.W., Trace Fossils: The relation of trace fossils to small scale sedimentary cycles in the British Lias. Special Issue Geological Journal (1970).

Silva, R.L., Duarte, L.V., Comas-Rengifo, M.J., Mendonca Filho, J.G., Azeredo, A.C., Update of the carbon and oxygen isotopic records of the Early–Late Pliensbachian (Early Jurassic, ~187 Ma): Insights from the organic-rich hemipelagic series of the Lusitanian Basin (Portugal). Chemical Geology 283, p. 177–184 (2011).

Silva, R.L., Duarte, L.V., Organic matter production and preservation in the Lusitanian Basin (Portugal) and Pliensbachian climatic hot snaps. Global and Planetary Change 131, p. 24–34 (2015).

Steinthorsdottir, M., Vajda, V., Early Jurassic (late Pliensbachian) CO_2 concentrations based on stomatal analysis of fossil conifer leaves from eastern Australia. Gondwana Research 27, no. 3, p. 932–939 (2013).

Steuber, T., Veizer, J., Phanerozoic record of plate tectonic control of seawater chemistry and carbonate sedimentation. Geology 30, no. 12, p. 1123–1126 (2002).

Suan, G., Mattioli, E., Pittet, B., Lecuyer, C., Sucheras-Marx, B., Duarte, L.V., Philippe, M., Reggiani, L., Martineau, F., Secular environmental precursors to Early Toarcian (Jurassic) extreme climate changes. Earth and Planetary Science Letters 290, p. 448–458 (2010).

Suan, G., Nikitenko, B.L., Rogov, M.A., Baudin, F., Spangenberg, J.E., Knyazev, V.G., Glinskikh, L.A., Goryacheva, A.A., Adatte, T., Riding, J.B., Follmi, K.B., Pittet, B., Mattioli, E., Lecuyer, C., Polar record of Early Jurassic massive carbon injection. Earth and Planetary Science Letters 312, p. 102–113 (2011).

Suan, G., Pittet, B., Bour, I., Mattioli, E., Duarte, L.V., Maillot, S., Duration of the Early Toarcian carbon isotope excursion deduced from spectral analyses: Consequence for its possible causes. Earth and Planetary Science Letters 267, p. 666–679 (2008).

Tappin, D. R, Chadwick, R. A, Jackson, A. A., Wingfield, R. T. R., Smith, N. J. P., Geology of Cardigan Bay and the Bristol Channel, United Kingdom Offshore Regional Report, British Geological Survey, HMSO, p. 107 (1994).

Ullmann, C.V., Hesselbo, S.P., Korte, C., Tectonic forcing of Early to Middle Jurassic seawater Sr/Ca. Geology 41, p. 1211–1214 (2013).

Ullmann, C.V., Thibault, N., Ruhl, M., Hesselbo, S.P., Korte, C., Effect of a Jurassic oceanic anoxic event on belemnite ecology and evolution. PNAS 111, no. 28, p. 10073–10076 (2014).

Van Buchem, F.P.S., Knox, R.W.O'B., Lower and middle Liassic depositional sequences of Yorkshire (UK). Mesozoic and Cenozoic Sequence Stratigraphy of European Basins, SEPM Special Publication No. 60 (1998).

Van Buchem, F.S.P., Melnyk, D.H., McCave, I.N., Chemical cyclicity and correlation of Lower Lias mudstones using gamma ray logs, Yorkshire, UK. Journal of the Geological Society 149, p. 991–1002 (1992).

Van Buchum, F.S.P., McCave, I.N., Cyclic sedimentation patterns in Lower Lias mudstones of Yorkshire (GB). Terra Nova 1, p. 461–467 (1989).

Van de Schootbrugge, B., Bailey, T.R., Rosenthal, Y., Katz, M.E., Wright, J.D., Miller, K.G., Feist-Burkhardt, S., Falkowski, P.G., Early Jurassic climate change and the radiation of organic- walled phytoplankton in the Tethys Ocean. Paleobiology 31, no. 1, p. 73-97 (2005).

Van der Meer, D.G., Zeebe, R.E., van Hinsbergen, D.J.J., Sluijs, A., Spakman, W., Torsvik, T.H., Plate tectonic controls on atmospheric CO_2 levels since the Triassic. PNAS 111, no. 12, p. 4380–4385 (2014).

Verati, C., Rapaille, C., feraud, G., Marzoli, A., Bertrand, H., Youbi, N., 40Ar/39Ar ages and duration of the central Atlantic Magmatic Province volcanism in Morocco and Portugal and its relation to the Triassic–Jurassic boundary. Palaeogeography, Palaeoclimatology, Palaeoecology 244, p. 308–325 (2007).

Von Hillebrandt, A.V., Krystyn, L., Kurschner, W.M., Bonis, N.R., Ruhl, M., Rochoz, S., Schobben, M.A.N., Urlichs, M., Bown, P.R., Kment, K., McRoberts, C.A., Simms, M., Tomasovych, A., The Global Stratotype Sections and Point (GSSP) for the base of the Jurassic System at Kuhjoch (Karwendel Mountains, Northern Calcareous Alps, Tyrol, Austrie). Episodes 36, no. 3, p. 162–198 (2013).

Waterhouse, H.K., Regular terrestrially derived palynofacies cycles in irregular marine sedimentary cycles, Lower Lias, Dorset, UK. Journal of the Geological Society, London 156, p. 1113–1124 (1999).

Weedon, G.P., Hemipelagic shelf sedimentation and climatic cycles: the basal Jurassic (Blue Lias) of South Britain. Earth and Planetary Science Letters 76, p. 321-335 (1985/86).

Weedon, G.P., Jenkyns, H.C., Coe, A.L., Hesselbo, S.P., Astronomical calibration of the Jurassic time-scale from cyclostratigraphy in British mudrock formations. Phil. Trans. R. Soc. Lond. A 357, p.1787–1813 (1999).

Weedon, G.P., Jenkyns, H.C., Cyclostratigraphy and the Early Jurassic timescale: Data from the Belemnite Marls, Dorset, southern England. Geological Society of America Bulletin 111, p. 1823–1840 (1999).

Weedon, G.P., the detection and illustration of regular sedimentary cycles using Walsh power spectra and filtering, with examples from the Lias of Switzerland. Journal of the Geological Society, London 146, p. 133–144 (1989).

Whiteside, J.H., Olsen, P.E., Eglinton, T., Brookfield, M.E., Sambrotto, R.,N., Compound-specific carbon isotopes from Earth's largest flood basalt eruptions directly linked to the end-Triassic mass extinction. PNAS 107, no. 15, p. 6721–6725 (2010).

Woodfine, R.G., Jenkyns, H.C., Sarti, M., Baroncini, F., Violante, C., The response of two Tethyan carbonate platforms to the Early Toarcian (Jurassic) oceanic anoxic event: environmental change and differential subsidence. Sedimentology 55, p. 1011–1028 (2008).

Woodland, A.W. (Ed.), The Llanbedr (Mochras Farm) Borehole. Institute of Geological Sciences Report 71, no. 18, p. 115 (1971).

Wotzlaw, J.-F., Guex, J., Bartolini, A., Gallet, Y., Krystyn, L., McRoberts, C.A., Taylor, D., Schoene, B., Schaltegger, U., Towards accurate numerical calibration of the Late Triassic: High-precision U-Pb geochronology constraints on the duration of the Rhaetian. Geology 42, no. 7, p. 571–574 (2014).

Figure 1

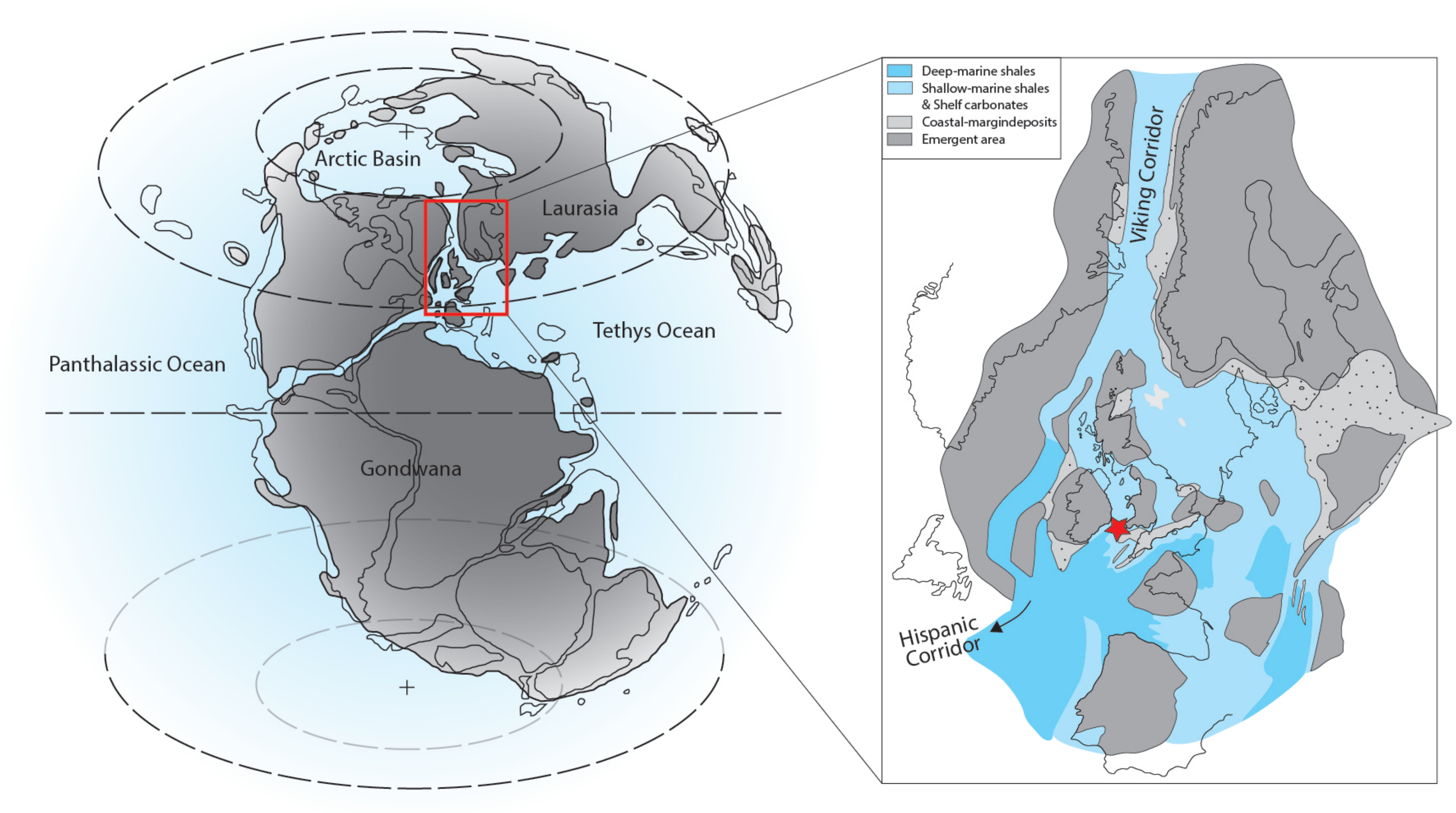
Arctic Basin
Laurasia
Tethys Ocean
Panthalassic Ocean
Gondwana
Deep-marine shales
Shallow-marine shales
& Shelf carbonates
Coastal-margindeposits
Emergent area
Viking Corridor
Hispanic
Corridor

Figure 2

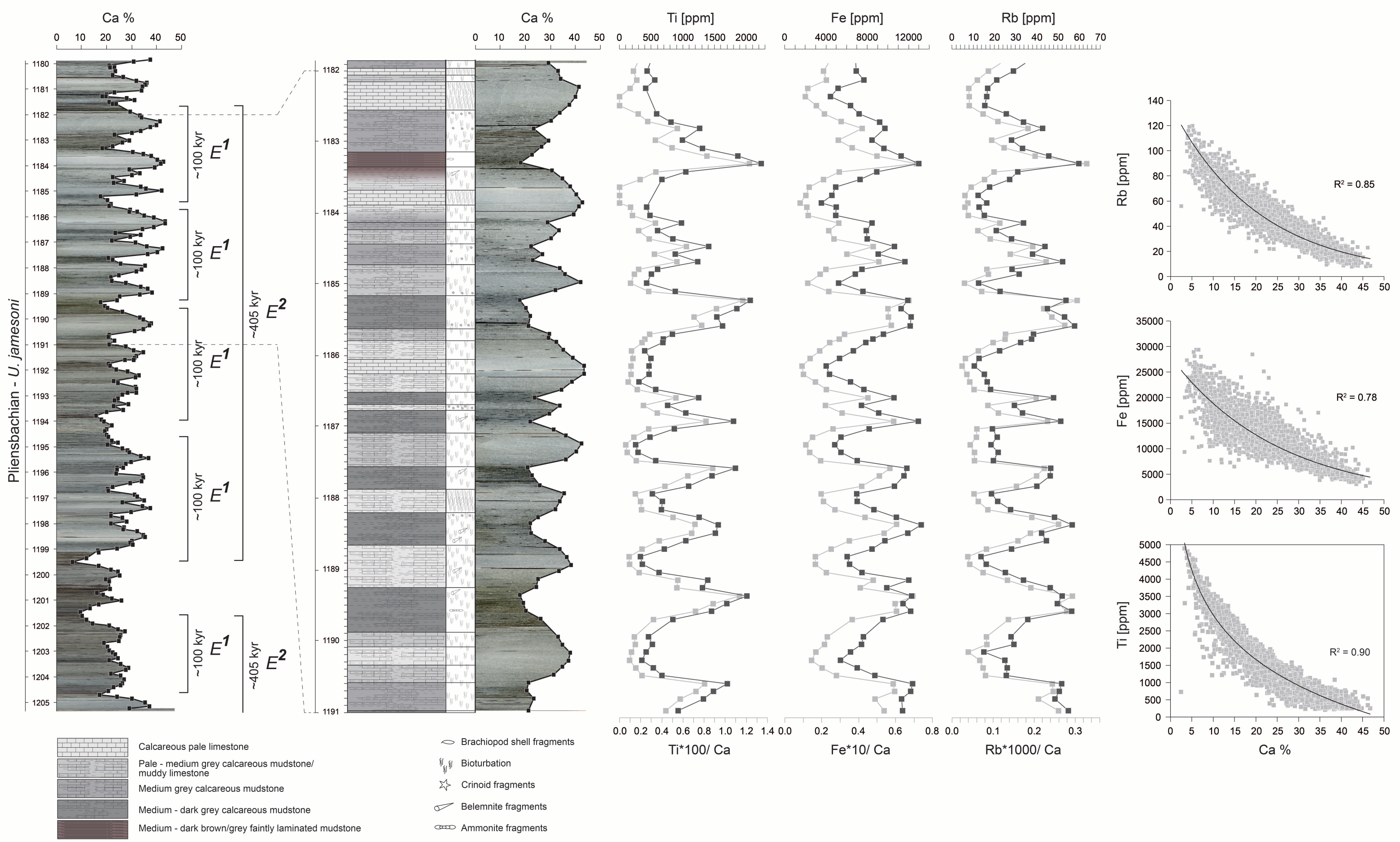

Pliensbachian - U. jamesoni
Ca %
~100 kyr E1
~405 kyr E2
Ti [ppm]
Fe [ppm]
Rb [ppm]
Ti*100/ Ca
Fe*10/ Ca
Rb*1000/ Ca
R² = 0.85
R² = 0.78
R² = 0.90
Calcareous pale limestone
Pale - medium grey calcareous mudstone/ muddy limestone
Medium grey calcareous mudstone
Medium - dark grey calcareous mudstone
Medium - dark brown/grey faintly laminated mudstone
Brachiopod shell fragments
Bioturbation
Crinoid fragments
Belemnite fragments
Ammonite fragments

Figure 3

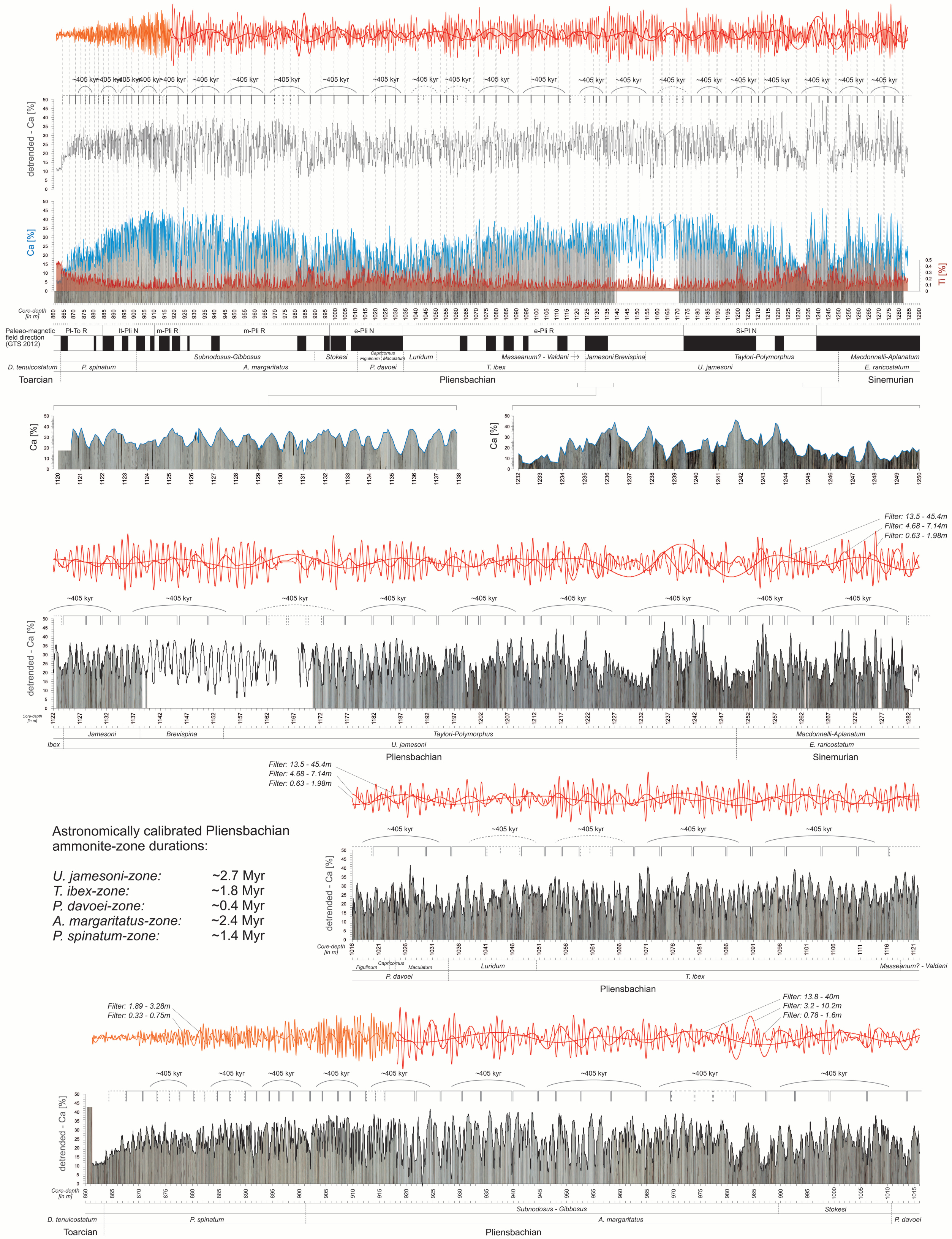

~405 kyr
detrended - Ca [%]
Ca [%]
Ti [%]
Core-depth [in m]
Palaeo-magnetic field direction (GTS 2012)
Pl-To R
lt-Pli N
m-Pli R
e-Pli N
e-Pli R
Si-Pl N
Subnodosus-Gibbosus
Stokesi
Capricornus
Figulinum
Maculatum
Luridum
Masseanum? - Valdani
Jamesoni
Brevispina
Taylori-Polymorphus
Macdonnelli-Aplanatum
D. tenuicostatum
P. spinatum
A. margaritatus
P. davoei
T. ibex
U. jamesoni
E. raricostatum
Toarcian
Pliensbachian
Sinemurian
Filter: 13.5 - 45.4m
Filter: 4.68 - 7.14m
Filter: 0.63 - 1.98m
Ibex
Astronomically calibrated Pliensbachian ammonite-zone durations:
U. jamesoni-zone: ~2.7 Myr
T. ibex-zone: ~1.8 Myr
P. davoei-zone: ~0.4 Myr
A. margaritatus-zone: ~2.4 Myr
P. spinatum-zone: ~1.4 Myr
Filter: 1.89 - 3.28m
Filter: 0.33 - 0.75m
Filter: 13.8 - 40m
Filter: 3.2 - 10.2m
Filter: 0.78 - 1.6m
Subnodosus - Gibbosus

Figure 4

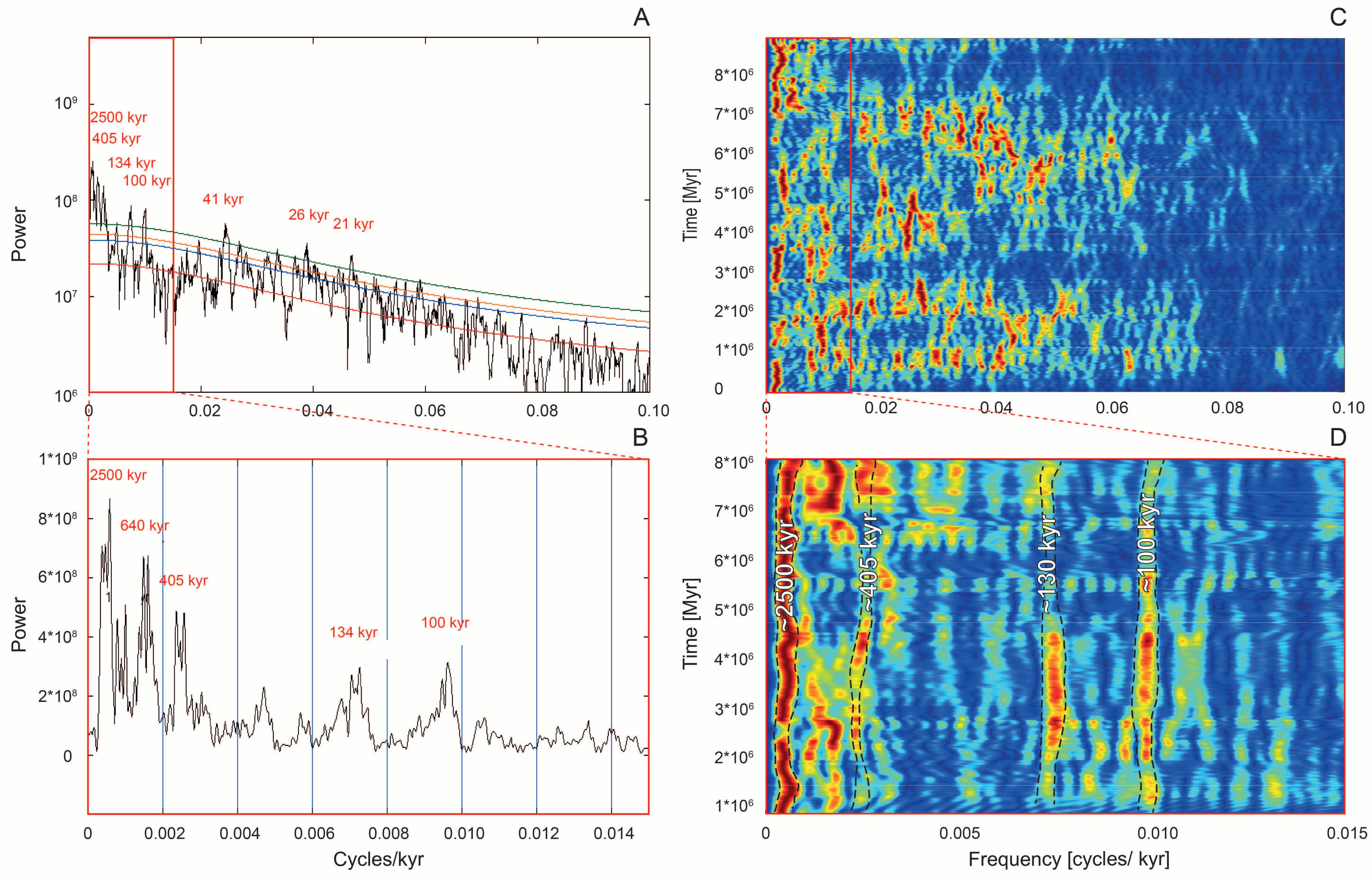
A
B
C
D
Power
2500 kyr
405 kyr
134 kyr
100 kyr
41 kyr
26 kyr
21 kyr
640 kyr
Cycles/kyr
Time [Myr]
~2500 kyr
~405 kyr
~130 kyr
~100 kyr
Frequency [cycles/ kyr]

Figure 5

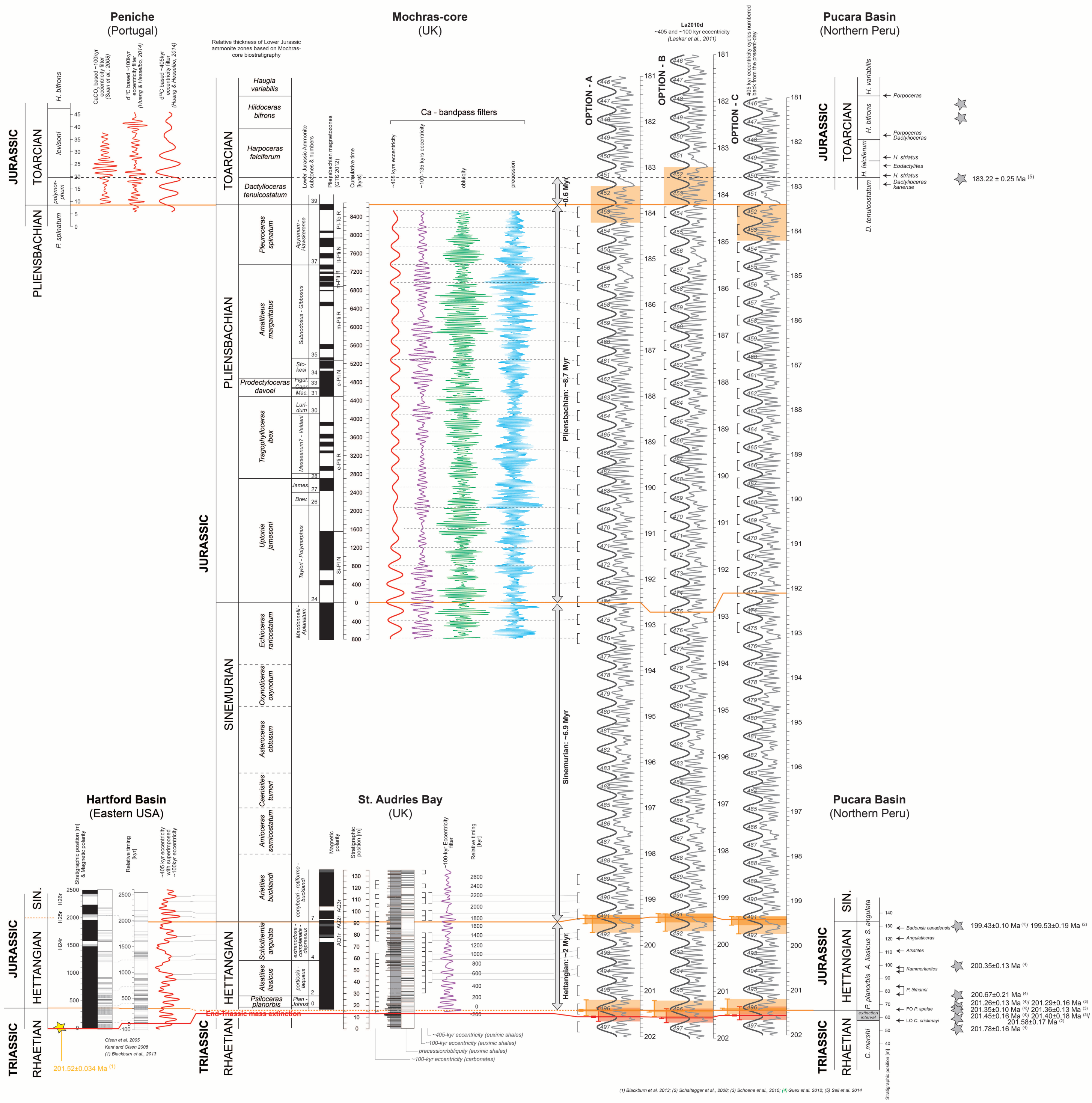

Peniche (Portugal)
Mochras-core (UK)
Pucara Basin (Northern Peru)
Hartford Basin (Eastern USA)
St. Audries Bay (UK)
OPTION - A
OPTION - B
OPTION - C
Ca - bandpass filters
JURASSIC
TRIASSIC
TOARCIAN
PLIENSBACHIAN
SINEMURIAN
HETTANGIAN
RHAETIAN
Pliensbachian: ~8.7 Myr
Sinemurian: ~6.9 Myr
Hettangian: ~2 Myr
End-Triassic mass extinction
183.22 ± 0.25 Ma (5)
199.43±0.10 Ma (4)/ 199.53±0.19 Ma (2)
200.35±0.13 Ma (4)
201.52±0.034 Ma (1)
(1) Blackburn et al. 2013; (2) Schaltegger et al., 2008; (3) Schoene et al., 2010; (4) Guex et al. 2012; (5) Sell et al. 2014

Figure 6

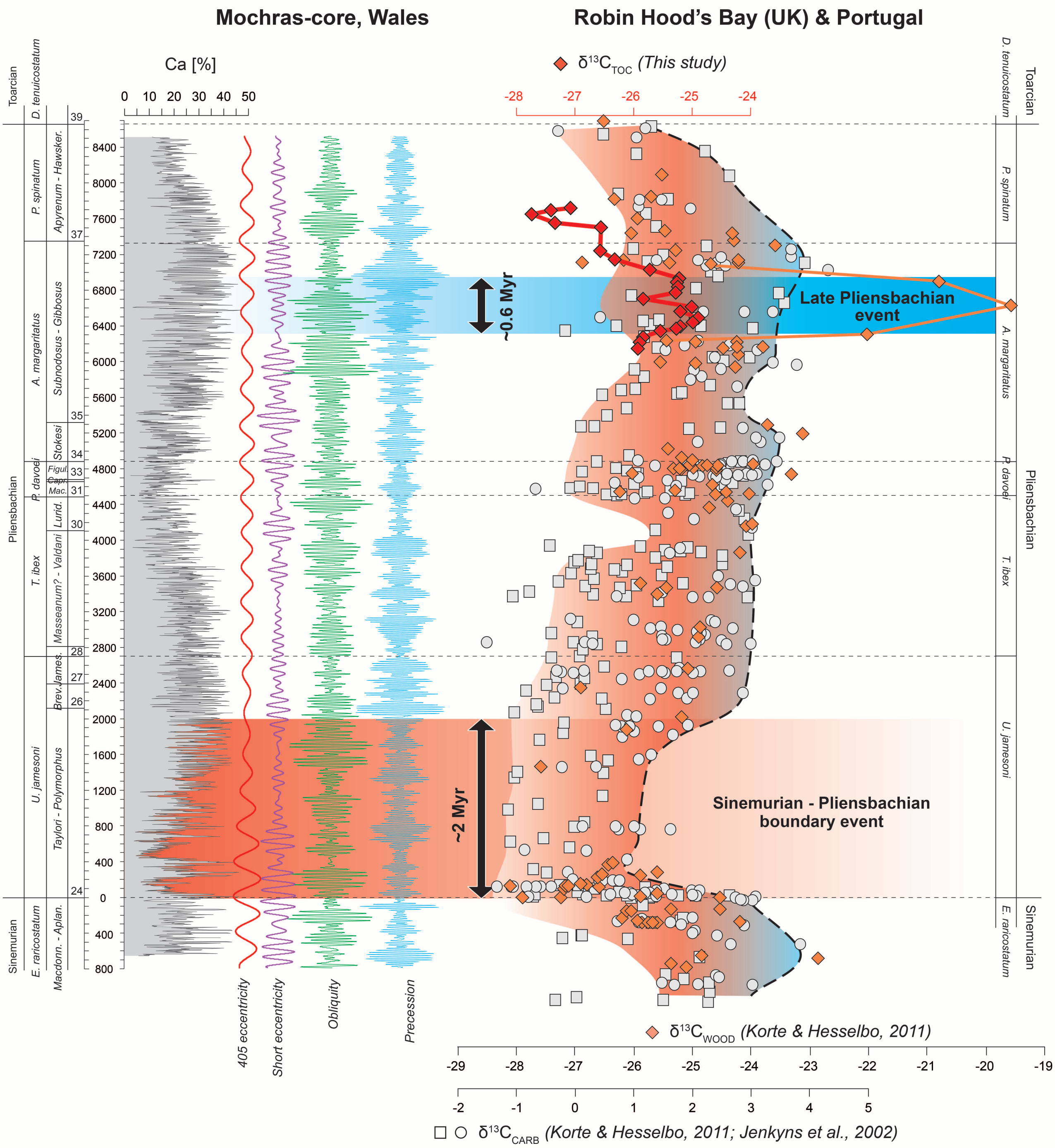

Mochras-core, Wales
Robin Hood's Bay (UK) & Portugal
Ca [%]
δ13C TOC (This study)
Late Pliensbachian event
~0.6 Myr
~2 Myr
Sinemurian - Pliensbachian boundary event
405 eccentricity
Short eccentricity
Obliquity
Precession
δ13C WOOD (Korte & Hesselbo, 2011)
δ13C CARB (Korte & Hesselbo, 2011; Jenkyns et al., 2002)
Toarcian
Pliensbachian
Sinemurian
D. tenuicostatum
P. spinatum
A. margaritatus
P. davoei
T. ibex
U. jamesoni
E. raricostatum
Apyrenum - Hawsker.
Subnodosus - Gibbosus
Stokesi
Taylori - Polymorphus
Macdonn. - Aplan.
Masseanum? - Valdani
Brev. James.

Figure 7

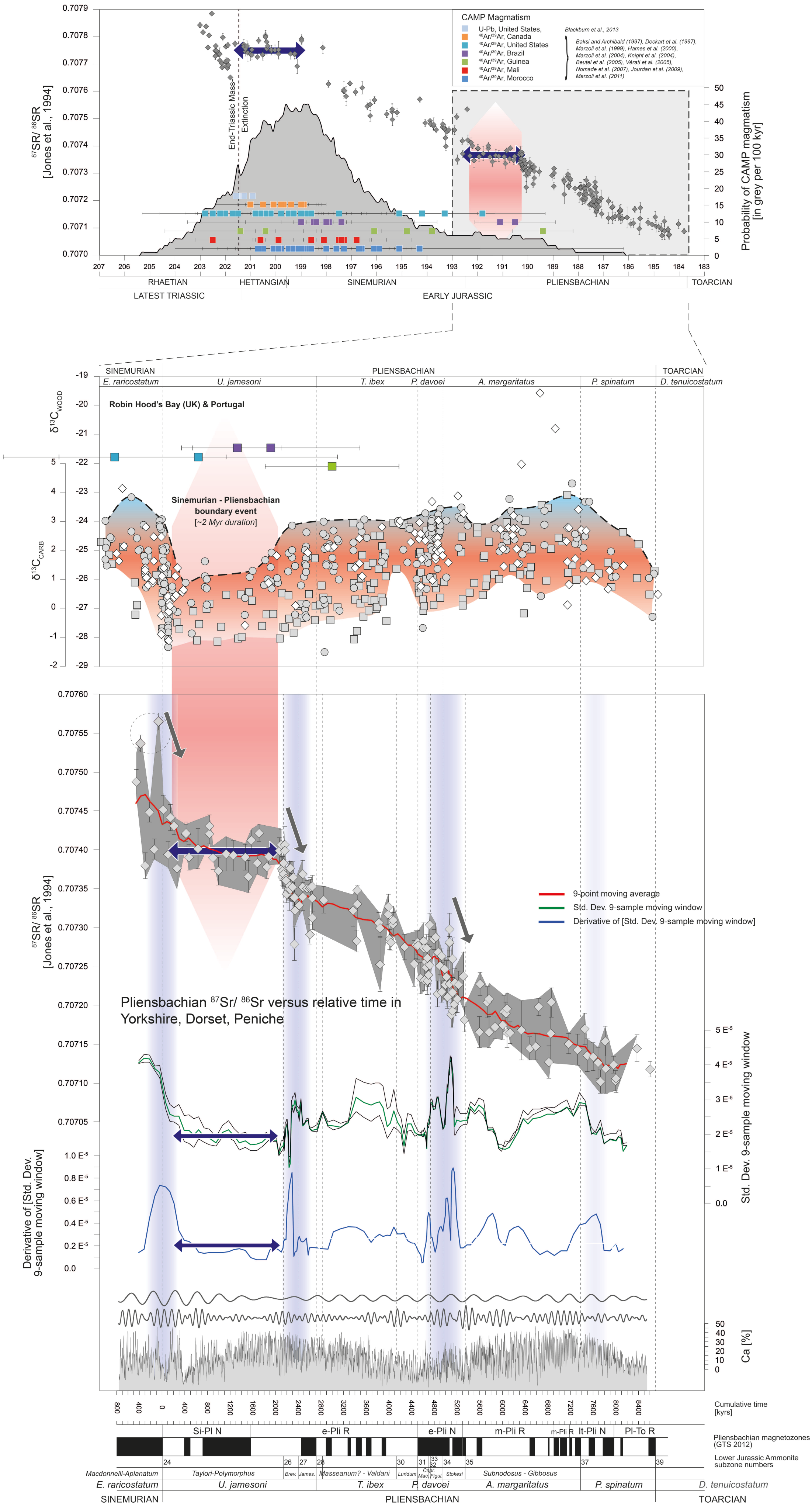

CAMP Magmatism
U-Pb, United States,
Blackburn et al., 2013
Robin Hood's Bay (UK) & Portugal
Sinemurian - Pliensbachian boundary event
[~2 Myr duration]
End-Triassic Mass-Extinction
Pliensbachian $^{87}Sr/^{86}Sr$ versus relative time in Yorkshire, Dorset, Peniche
9-point moving average
Std. Dev. 9-sample moving window
Derivative of [Std. Dev. 9-sample moving window]
$^{87}Sr/^{86}SR$ [Jones et al., 1994]
Probability of CAMP magmatism [in grey per 100 kyr]
Std. Dev. 9-sample moving window
Derivative of [Std. Dev. 9-sample moving window]
Ca [%]
Cumulative time [kyrs]
Pliensbachian magnetozones (GTS 2012)
Lower Jurassic Ammonite subzone numbers
RHAETIAN
HETTANGIAN
SINEMURIAN
PLIENSBACHIAN
TOARCIAN
LATEST TRIASSIC
EARLY JURASSIC
E. raricostatum
U. jamesoni
T. ibex
P. davoei
A. margaritatus
P. spinatum
D. tenuicostatum

Table 1: Lower Jurassic Stage and Ammonite Zone Ages and Durations

Stage	Ammonite Zone	Base Age [Myr]	Duration [Myr]
	tenuicostatum	183.8 +/- 0.4	~0.6
Toarcian		**183.8 +/- 0.4**	**~8.3**
	spinatum	185.2 +/- 0.4	~1.4
	margaritatus	187.6 +/- 0.4	~2.4
	davoei	188.0 +/- 0.4	~0.4
	ibex	189.8 +/- 0.4	~1.8
	jamesoni	192.5 +/- 0.4	~2.7
Pliensbachian		**192.5 +/- 0.4**	**~8.7**
	raricostatum		> 0.8
	oxynotum		
	obtusum		
	turneri		
	semicostatum		
	bucklandi	199.43 +/- 0.1	> 1.1
Sinemurian		**199.43 +/- 0.1**	**6.93 +/- 0.5**
	angulata	~200.25	~0.82
	liasicus	~201.04	~0.79
	planorbis	~201.35	~0.31
Hettangian		**201.42 +/- 0.02**	**1.99 +/- 0.12**

Supplementary Figure 1

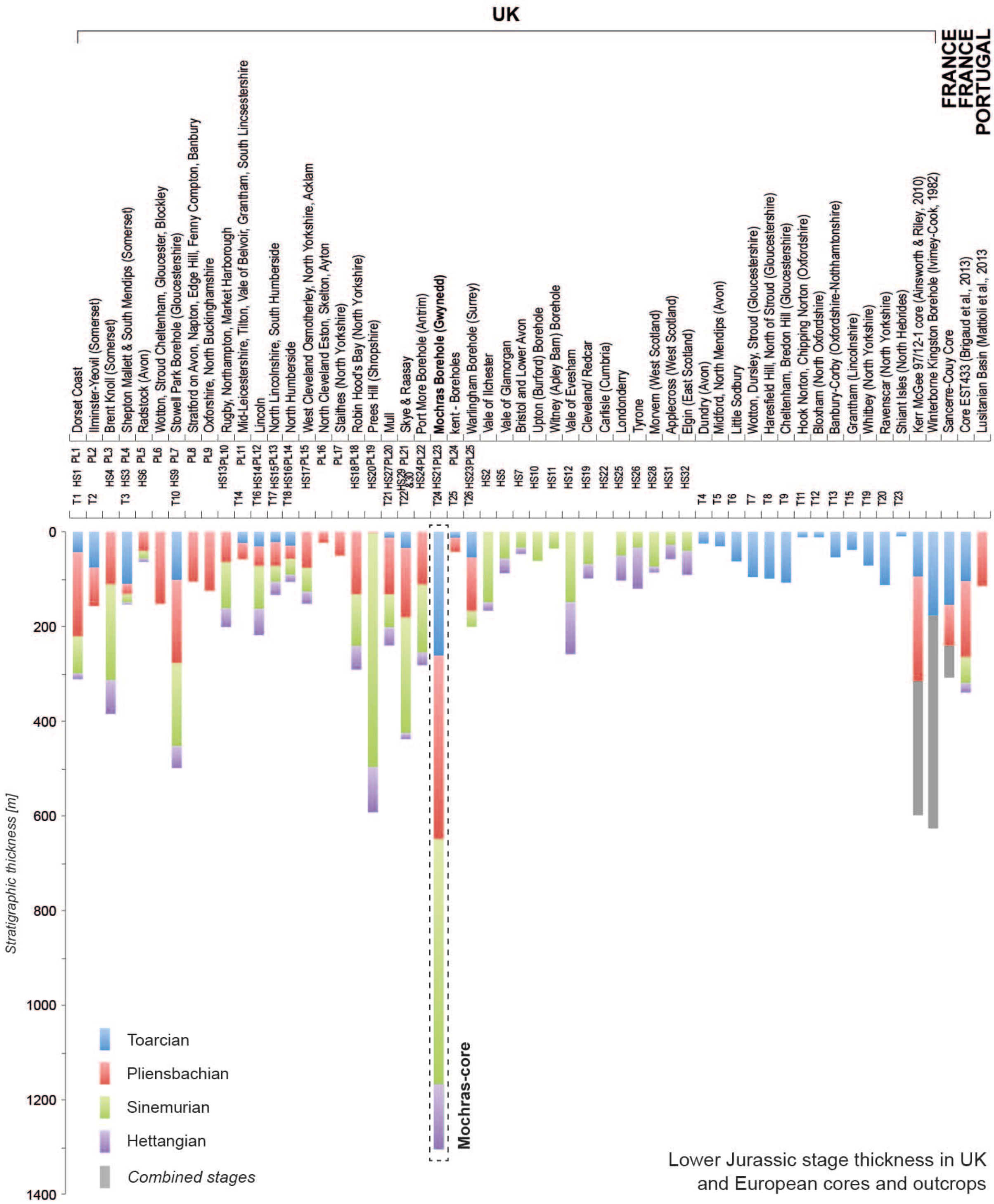

Supplementary Figure 2

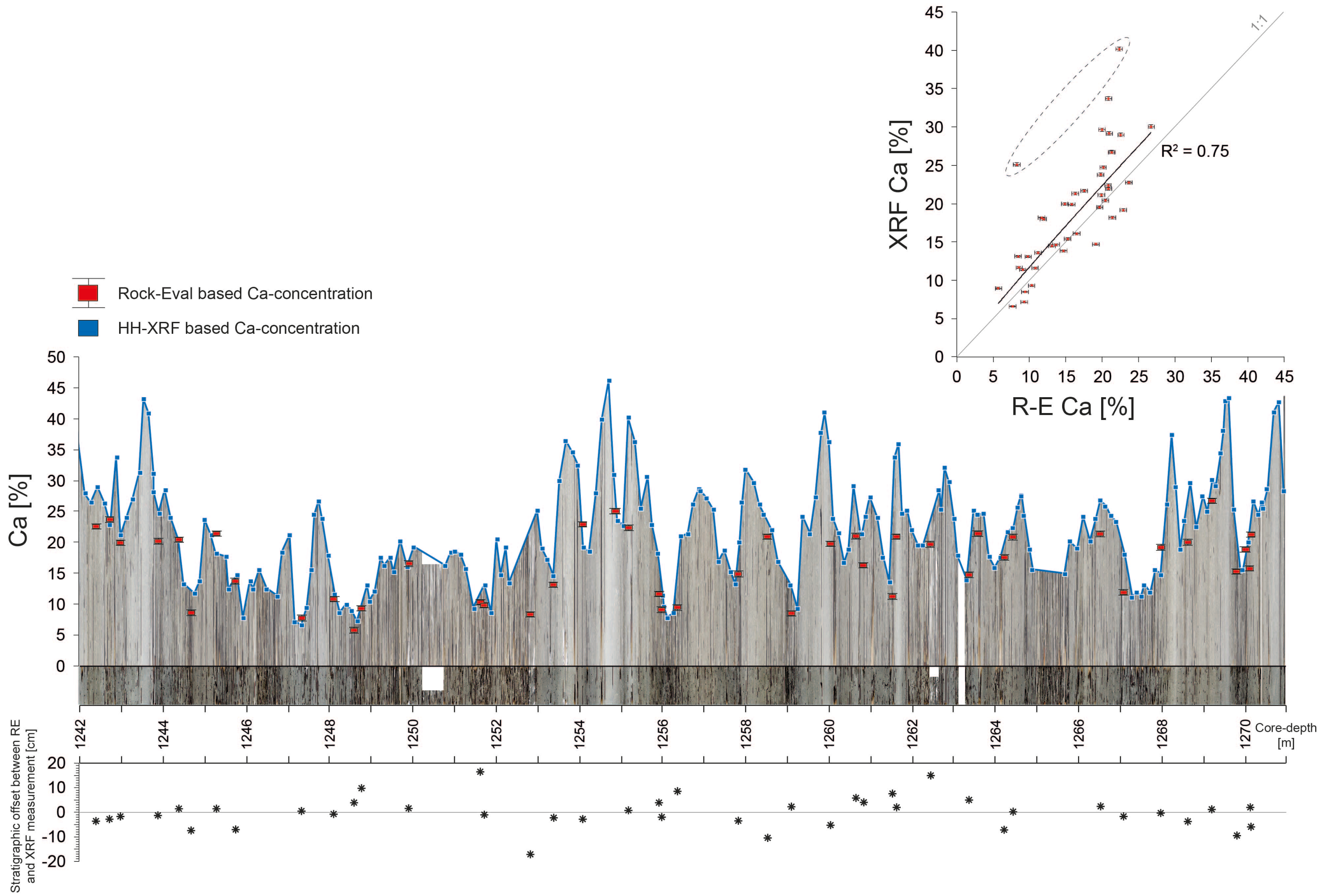

Supplementary Figure 3

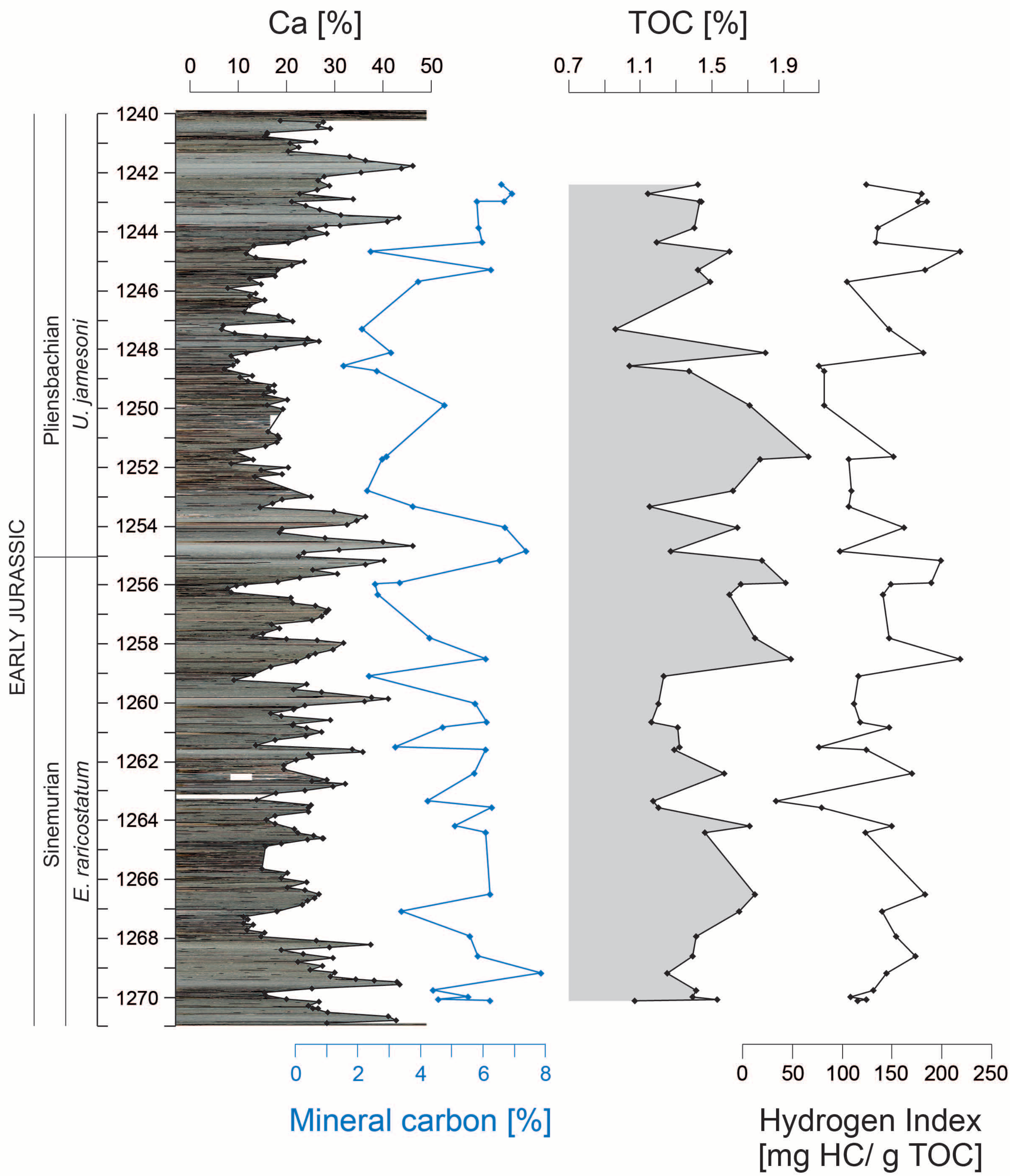

Supplementary Figure 5

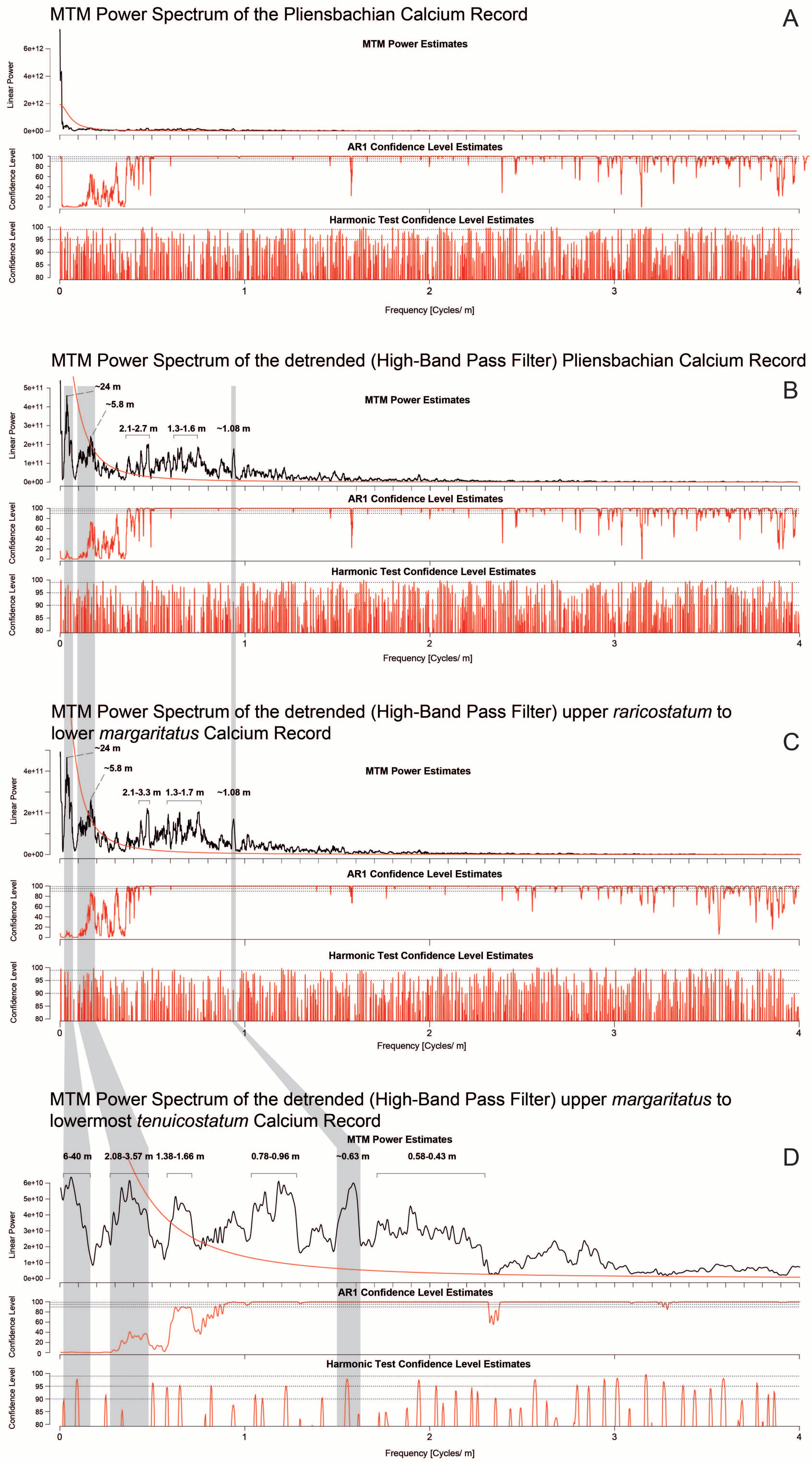

Supplementary Figure 6

Fe [high bandpass filter]

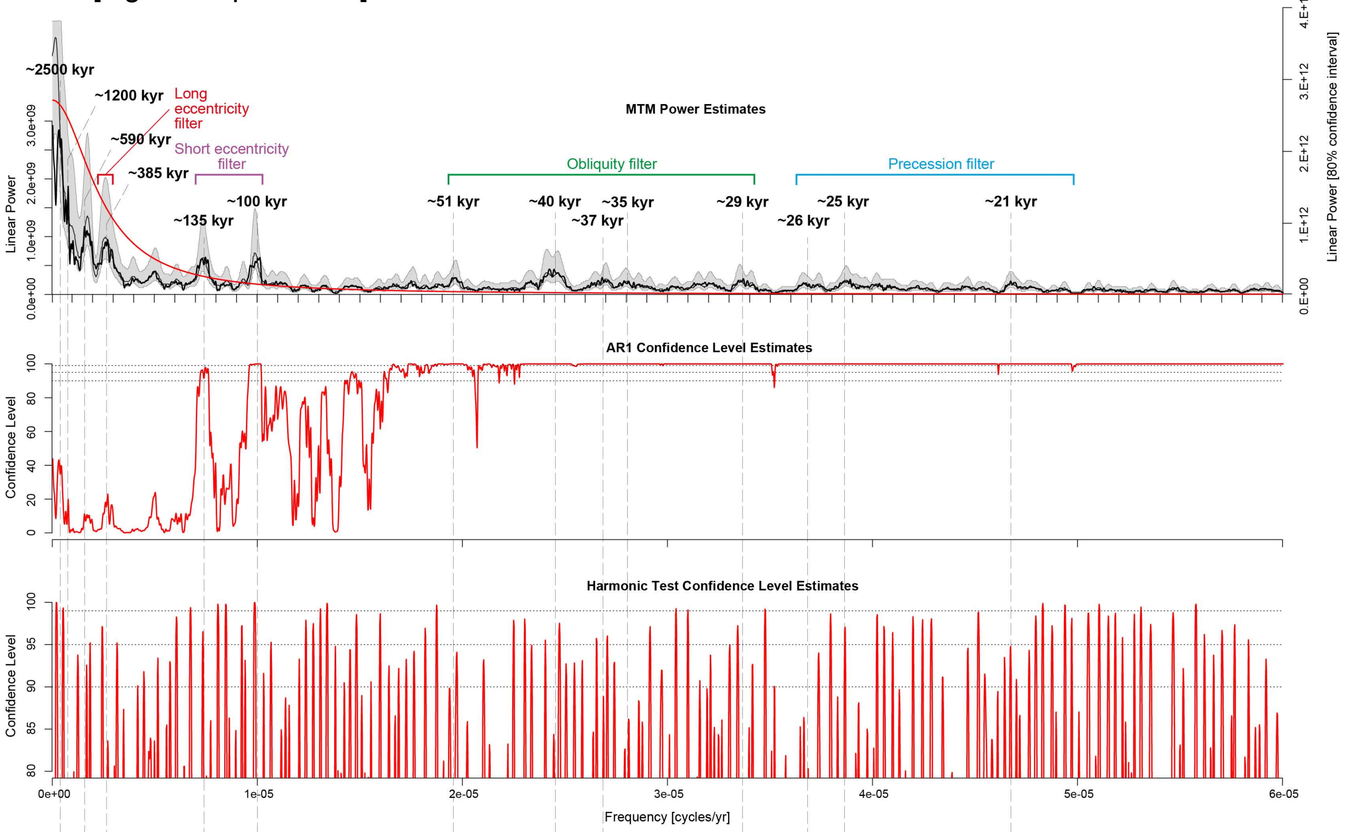

Ca [high bandpass filter]

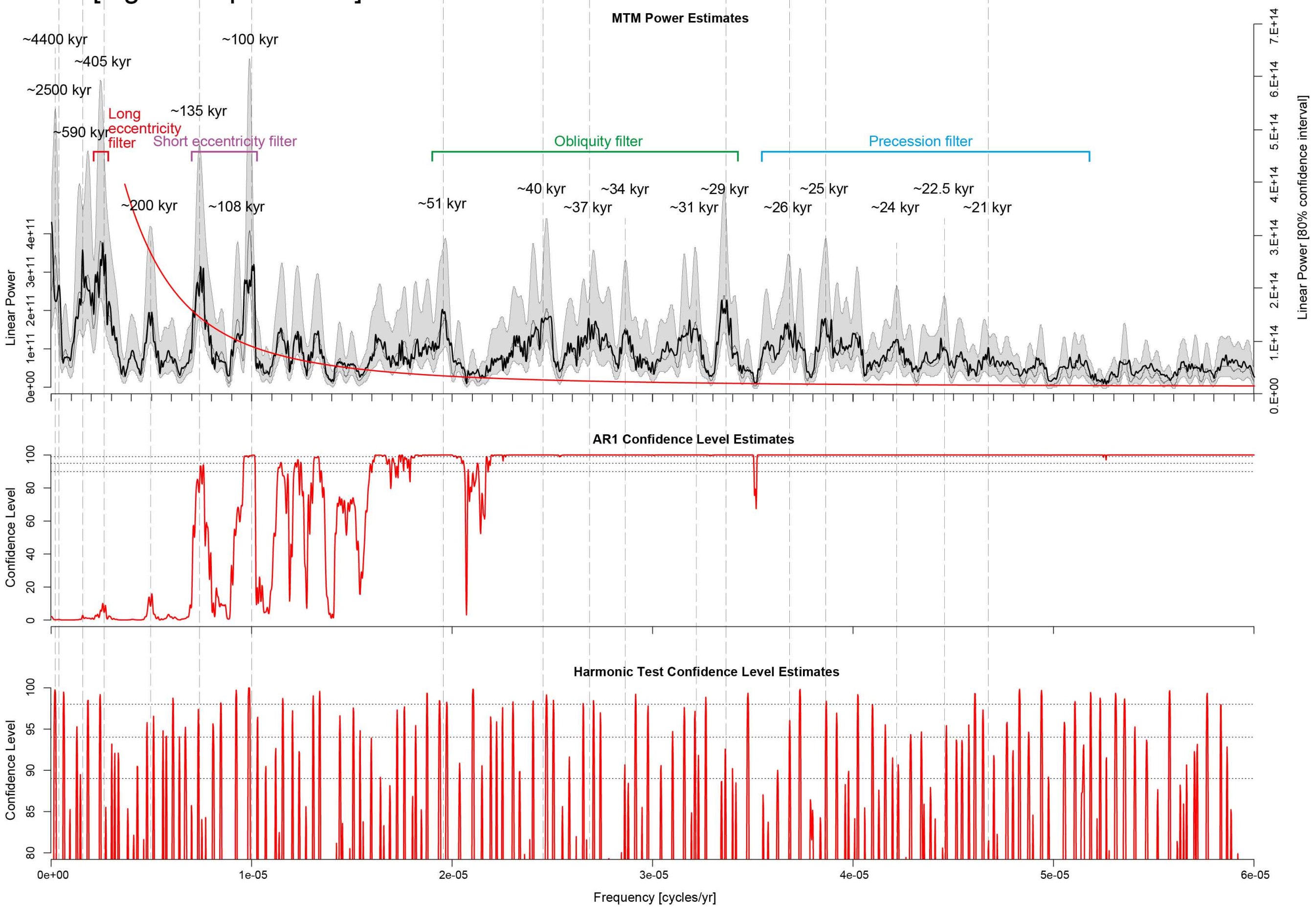

Supplementary Figure 7

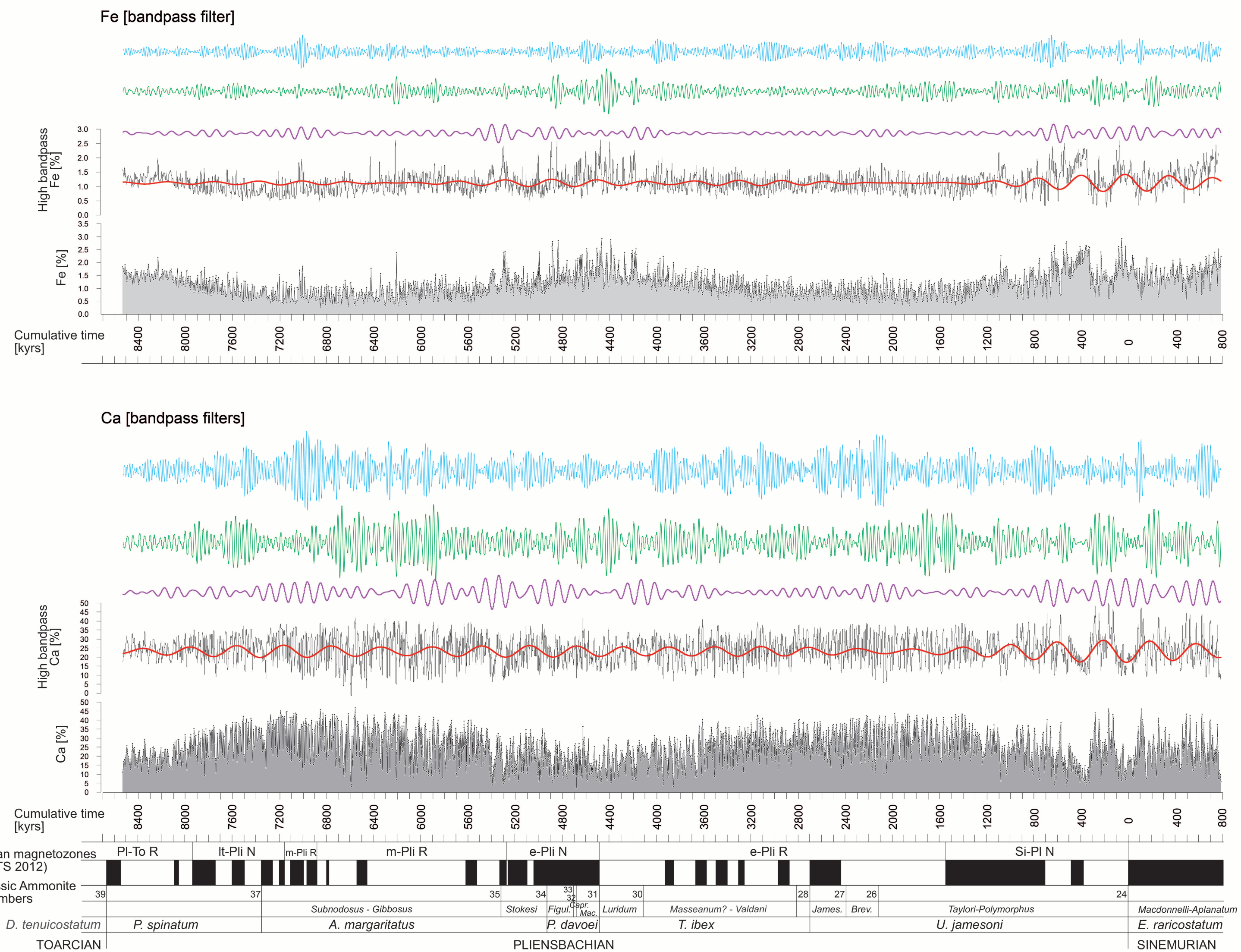

Supplementary Figure 8